Fakultät für Medizin

Histologically confirmed diagnostic efficacy of ^{18}F-rhPSMA-7 PET for staging of patients with primary high-risk prostate cancer

Lena Kristin Jooß

Vollständiger Abdruck der von der Fakultät für Medizin der Technischen Universität München zur Erlangung einer Doktorin der Medizin genehmigten Dissertation.

Vorsitz: apl. Prof. Dr. Stefan Thorban

Prüfer der Dissertation:

1. Prof. Dr. Tobias Maurer
2. Priv.-Doz. Dr. Edouard Matevossian

Die Dissertation wurde am 14.02.2022 bei der Technischen Universität München eingereicht und durch die Fakultät für Medizin am 12.07.2022 angenommen.

Klinikum rechts der Isar
Department of Nuclear Medicine
Mentoring: Prof. Dr. Maurer and Prof. Dr. Eiber

Histologically confirmed diagnostic efficacy of ^{18}F-rhPSMA-7 PET for staging of patients with primary high-risk prostate cancer

Lena Kristin Jooß

Full version of a thesis submitted for the degree of Dr. med. at the Technical University Munich, 14th February 2022

Acceptance by the Faculty of Medicine, 12th July 2022

Chair of the oral examination: Prof. Dr. Stefan Thorban
Examiner: Prof. Dr. Tobias Maurer and PD Dr. Edouard Matevossian

With thanks for the highly appreciated work and help of Matthias Eiber as well as of Markus Krönke, Alexander Wurzer, Kristina Schwamborn, Lena Ulbrich, Tobias Maurer, Saskia Kropf, Thomas Horn, Bernhard Haller, Hans-Jürgen Wester and Wolfgang Weber.

Please note that this thesis and scientific issue were based on the same dataset and working group as the paper of Markus Krönke (Krönke et al., 2020) leading to similarities in data presentation.

Outline

List of figures

List of tables

List of abbreviations (alphabetical)

AS: Active surveillance

AUC: area under the curve

AWMF: Arbeitsgemeinschaft der Wissenschaftlichen Medizinischen Fachgesellschaften

CI: confidence interval

CSS: Cancer specific survival

CT: computer tomography

DRE: Digital rectal examination

ERSPC: European Randomized Study of Screening for Prostate Cancer

F: Fluor

FDA: Food and Drug Administration

FDG: Fluorodeoxyglucose

Ga: Gallium

GEE: generalized-estimating-equation

GS: Gleason score

IC50: half maximal inhibitory concentration

IQR: interquartile range

LNCaP: lymph node carcinoma of the prostate, a cell line originating from a metastatic lesion of human prostatic adenocarcinoma used for research about prostate cancer

LOR: Line of response

MRI: magnetic resonance imaging

mpMRI: multi parametric magnetic resonance imaging

OS: overall survival

PACS: Picture Archiving and Communication System

PCa: Prostate Carcinoma

PET: Positron-Emission-Tomography

PLCO: group for the Prostate, Lung, Colorectal and Ovarian screening trial

PLND: Pelvic lymph node dissection

PPV: positive predictive value

PSA: Prostate specific antigen

PSMA: Prostate specific membrane antigen

RALP: Robot-assisted laparoscopic radical prostatectomy

rhPSMA: radiohybrid prostate specific antigen

ROC: receiver-operating-characteristic

RP: Radical prostatectomy

RRP: retropubic radical prostatectomy

RT: Radiation therapy

SiFA: Silicon-Fluoride-Acceptor

UICC: Union for international cancer control

WW: Watchful waiting

Abstract

Purpose: ^{18}F-rhPSMA-7 is a new PSMA (prostate specific membrane antigen)-targeting agent with the advantage of both efficient labelling with ^{18}F and radiometals and a minimal renal excretion. This retrospective analysis investigates the diagnostic efficacy of ^{18}F-rhPSMA-7 PET for lymph node staging compared to morphological imaging (CT and MRI) for patients with primary high-risk prostate cancer, validated by histopathology.

Methods: Data from 58 patients with high-risk prostate cancer (defined by D'Amico) who were staged with ^{18}F-rhPSMA-7 PET/CT or PET/MRI between July 2017 and June 2018 was analysed. Median pre-scan PSA was 12.4 ng/mL (range, 1.2–81.6 ng/ml). Median injected activity of ^{18}F-rhPSMA-7 was 327 MBq (range, 132–410 MBq), with a median uptake time of 79.5 min (range, 60–153 min). All patients underwent subsequent radical prostatectomy and extended pelvic lymph node dissection. PET and morphological datasets were rated independently by an experienced reader for the presence of lymph node metastases. Results were compared to histopathological findings on a patient- and template-based manner.

Results: Lymph node metastases were present in 18 patients (31.0%) located in 52 of 375 templates (13.9%). On patient-based analyses ^{18}F-rhPSMA-7 PET showed a sensitivity of 72.2%, a specificity of 92.5% and an accuracy of 86.2%. Morphological imaging resulted in 50.0%, 72.5% and 65.5%, respectively. On template-based analyses the sensitivity, specificity and accuracy of ^{18}F-rhPSMA-7 PET were 53.8%, 96.9% and 90.9%, and those of morphological imaging were 9.6%, 95.0% and 83.2%, respectively. ROC analyses showed ^{18}F-rhPSMA-7 PET to perform significantly better than morphological imaging on both patient (AUCs of 0.858 vs. 0.649, p=0.012) and template-based analyses (AUCs of 0.766 vs. 0.589, p<0.001). Median histopathological size of lymph node metastases missed in ^{18}F-rhPSMA-7 was 3.5 mm (range, 0.3–15 mm).

Conclusion: ^{18}F-rhPSMA-7 PET is superior to morphological imaging for lymph node staging of high-risk primary prostate cancer. Its diagnostic efficacy is similar to published data for other PSMA-ligands.

Introduction

The prostate is an exocrine accessory sex gland enclosing the prostatic urethra which joins the paired ejaculatory ducts. It can be divided into five zones (defined by McNeal (1981)) which are the peripheral, central, transition, anterior and periurethral zone, see Figure 1. It produces about 30% of the ejaculate volume, secreting an acid liquid, which contains a lot of phosphatases, especially acid phosphatase (Schulte, 2020).

Figure 1: *Prostate zones*

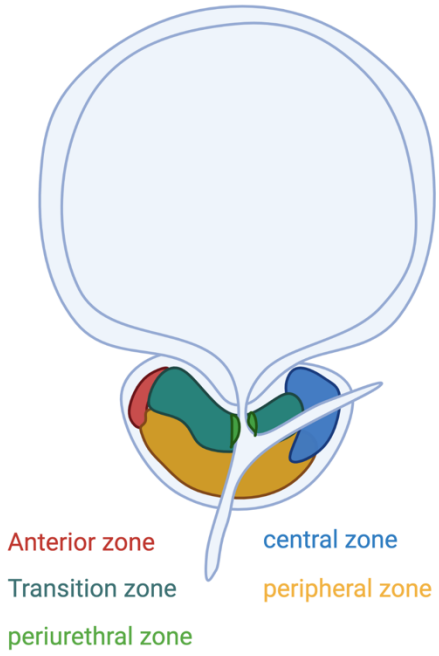

Note. The prostate can be divided into five zones (defined by McNeal (1981)): the anterior, transition, periurethral, central and peripheral zone. Figure created with BioRender.com (n.d.), adapted from (amboss.com, 2020).

Prostate Carcinoma

Relevance

Worldwide prostate carcinoma (PCa) is the second most frequently diagnosed cancer in men, in developed countries it is the most frequently diagnosed cancer in men. In Germany there are about 60 000 men each year diagnosed with prostate cancer. Looking at leading

causes of cancer death, prostate cancer is on the fifth place worldwide and with 11,3% on the second place in Germany with about 12 000 men dying each year because of the disease and its consequences (AWMF online, 2019; Torre et al., 2015). Age standardized disease rate in Germany is stable since 2003 and decreasing since 2011. Age standardized death rate is stable since 2017 (Zentrum für Krebsregisterdaten und Gesellschaft der epidemiologischen Krebsregister in Deutschland e.V., 2017).

Risk factors

Well-established risk factors are age and family history. Concerning age, the risk of a 35-year old man to come down with prostate cancer in the next ten years is less than 0,1 %, whereas the risk of a 75-year old man is about 5% (Zentrum für Krebsregisterdaten und Gesellschaft der epidemiologischen Krebsregister in Deutschland e.V., 2017).
With one first-degree relative suffering from PCa the risk is doubled and it is five to eleven times higher with two or more first-line relatives being affected (Hemminki, 2012; Mottet et al., 2017). About 9% of patients with PCa have a hereditary disease, which leads to an early onset (6-7 years earlier) of the disease. Carriers of BRCA2 germline abnormality also show an early onset and also a more aggressive tumour behaviour (Castro et al., 2013; Mottet et al., 2017). A connection between metabolic syndrome and PCa is discussed, but the metanalysis of Esposito et al. (2013) only found a significant association in studies for Europe but not for the US or Asian countries. Independent from geography, they found a significant association between hypertension and PCa.

Classification

Histological origin

With 95% Adenocarcinomas are the most common histological type of PCa. Typically they originate from peripheral zones of the prostate from acinar and proximal duct epithelium (Ferreira et al., 2015).

Grading

The most common used grading system is the Gleason Grading system, which analyses the architectural pattern of the tumour, see Figure 2. 1 stands for simple round glands, close-

packed in rounded masses with well-defined edges, 2 stands for simple rounded glands loosely packed in vague, rounded masses with loosely defined edges, 3 stands for medium sized single glands of irregular shape and irregular spacing with ill-defined infiltrating edges, 4 stands for small, medium, or large glands fused into cords, chains, or ragged, infiltrating masses and 5 stands for papillary and cribriform epithelium in smooth, rounded masses, with central necrosis (Gleason, 1992). The Gleason Score (GS) of a biopsy consists of the Gleason grade of the most extensive pattern plus the highest pattern (with the least differentiation). The GS of radical prostatectomy (RP) is defined as the sum of the most common grade pattern plus the second most common grade pattern (Ferreira et al., 2015; Mottet et al., 2017; Paul et al., 2008).

Figure 2: *Gleason standard drawing*

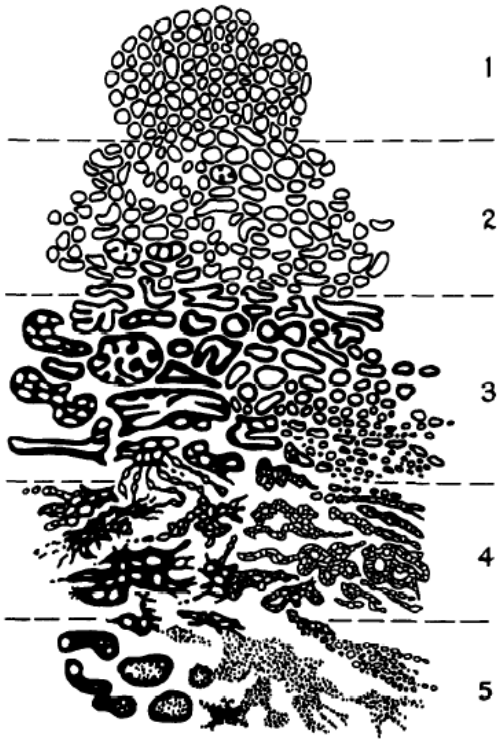

Note. Gleason's architectural patterns: 1: simple round glands, close-packed in rounded masses with well-defined edges, 2: simple rounded glands loosely packed in vague, rounded masses with loosely defined edges, 3: Medium sized single glands of irregular shape and irregular spacing with ill-defined infiltrating edges, 4: small, medium, or large glands fused into cords, chains, or ragged, infiltrating masses, 5: Papillary and cribriform epithelium in smooth, rounded masses, with central necrosis (Gleason, 1992).

TNM classification

The TNM classification is used for the staging of the PCa. “T” in TNM is categorizing tumour size and local tumour extension. “N” regional lymph node metastases and “M” distant metastases.

Regional lymph nodes include all pelvic lymph nodes below the bifurcation of the common iliac arteries: pelvic, hypogastric, obturator, iliac, and sacral lymph nodes (Buyyounouski et al., 2017).

Distant metastases can be found most often in bones, lung and liver. Bone metastases show the highest frequency and occur earlier than lung and liver metastases (Bubendorf et al., 2000; Buyyounouski et al., 2017).

It can be differentiated between a clinical and a pathological classification. For clinical classification digital rectal examination (DRE) and imaging processes are used. The pathological classification can be made after radical prostatectomy and pelvic lymph node dissection (PLND) (Buyyounouski et al., 2017) (see Table 1).

Table 1: *Definitions of American Joint Committee on Cancer TNM Criteria*

Category	Criteria
Clinical (cT)	
T category	
TX	Primary tumour cannot be assessed
T0	No evidence of primary tumour
T1	Clinically inapparent tumour that is not palpable
T1a	Tumour incidental histologic finding in 5% or less of tissue resected
T1b	Tumour incidental histologic finding in more than 5% of tissue resected
T1c	Tumour identified by needle biopsy found in one or both sides, but not palpable
T2	Tumour is palpable and confined within prostate
T2a	Tumour involves one-half of one side or less
T2b	Tumour involves more than one-half of one side but not both sides
T2c	Tumour involves both sides
T3	Extraprostatic tumour that is not fixed or does not invade adjacent structures

T3a	Extraprostatic extension (unilateral or bilateral)
T3b	Tumour invades seminal vesicle(s)
T4	Tumour is fixed or invades adjacent structures other than seminal vesicles, such as external sphincter, rectum, bladder, levator muscles, and/or pelvic wall
Pathologic (pT)	
T category	
T2	Organ confined
T3	Extraprostatic extension
T3a	Extraprostatic extension (unilateral or bilateral) or microscopic invasion of bladder neck
T3b	Tumour invades seminal vesicle(s)
T4	Tumour is fixed or invades adjacent structures other than seminal vesicles, such as external sphincter, rectum, bladder, levator muscles, and/or pelvic wall
N category	
NX	Regional lymph nodes were not assessed
N0	No positive regional lymph nodes
N1	Metastases in regional lymph node(s)
M category	
M0	No distant metastasis
M1	Distant metastasis
M1a	Nonregional lymph node(s)
M1b	Bone(s)
M1c	Other site(s) with or without bone disease

Note. TNM classification, "T" in TNM is categorizing tumour size and local tumour extension, "N" regional lymph node metastases and "M" distant metastases.
Table from Buyyounouski et al. (2017).

In the UICC (Union for international cancer control) classification the TNM states can be summarized as locally limited prostate cancer (Stage I: T1, T2a, N0, M0 and Stage II: T2b,

T2c, N0, M0), locally advanced prostate cancer (Stage III: T3, T4, N0, M0) and advanced or metastasized prostate cancer (Stage IV: Any T, N1, M0 or any T, any N and M1) (AWMF online, 2021; Brierley, Gospodarowicz, & Wittekind, 2017).

Diagnostic Process

Diagnostic tools for diagnosing a PCa are the measurement of PSA-Level, a digital rectal examination (DRE) and taking a biopsy as gold standard to determine the Gleason Score and T-stage of TNM classification. These parameters except for DRE are also used to classify patients in low, intermediate and high risk. For the staging different imaging methods are available such as MRI, CT, PET and skeletal scintigraphy. The guidelines (AWMF online, 2019) recommended PET imaging only for controlled clinical studies.
In the year 2021 the guidelines were adjusted. As the applicable ones during this study were from 2019 those will be the point of reference for this thesis.
The new guidelines from 2021 (AWMF online, 2021) state a higher diagnostic accuracy for metastases of PSMA-PET over CT in combination with skeletal scintigraphy. Therefore it states PSMA-PET/CT can be used for the staging of high-risk prostate cancer. Furthermore, the new guidelines recommend PSMA-PET hybrid imaging for recurrent prostate cancer as first choice. But a negative PSMA-PET must not delay salvage therapy (AWMF online, 2021).

Prostate specific Antigen

The prostate specific antigen (PSA) is a serine protease, which liquifies the ejaculate. It is produced in prostatic epithelial cells and increases in PCa. A higher PSA level indicates a higher risk of prostate cancer, but testing should always take place in the same laboratory due to missing standards and an isolated increase in PSA must be confirmed with a second testing a few weeks later to exclude other explanations of an increase such as ejaculation, manipulation or urinary tract infections (Mottet et al., 2017; Paul et al., 2008).
There is a critical discussion about the benefit of PSA screening for PCa. A review from Hayes and Barry (2014) showed an increased cancer incidence in the screening group for the Prostate, Lung, Colorectal and Ovarian (PLCO) screening trial and the European Randomized Study of Screening for Prostate Cancer (ERSPC). Though only the ERSPC showed a reduced risk of prostate cancer mortality after 11 years, whereas the PLCO found no mortality benefit in a 13-year follow up (Hayes & Barry, 2014). A review of 2018 showed a significant mortality

benefit in a European trial (Fenton et al., 2018). Harms of overdiagnosis and overtreatment lead to a strong advice against a systematic population-based PSA-screening. Therefore there is only a Level A recommendation for PSA screening for men with an elevated risk of PCa: men aged > 50 years, men aged >45 years and family history, African American men aged >45 years, men with PSA level >1 ng/ml at age 40 and men with a PSA level >2 ng/ml at age 60 (Mottet et al., 2017). There is also a consensus about stopping screening in patients with a life expectancy smaller than 15 years (Mottet et al., 2017). Continuing the diagnostic process with biopsy is recommended for PSA levels higher than 4 ng/ml or a suspicious PSA increase (AWMF online, 2019).

Digital rectal examination

There is a level B recommendation for a digital rectal examination (DRE) additional to a PSA test, if the patient wishes a screening after receiving information about the benefits and disadvantages of screenings (AWMF online, 2019). Although the PSA score is a better predictor of prostate cancer DRE still should be used to detect PSA-negative PCa (Mottet et al., 2017; Paul et al., 2008). In accordance with the American Joint Committee on Cancer the clinical T classification should only consider information from DRE (Buyyounouski et al., 2017). Suspicious palpatory findings are an indication for prostate biopsy (AWMF online, 2019).

Biopsy

The AWMF guideline for PCa (AWMF online, 2019) recommends a transrectal ultrasound-guided core-needle biopsy with 10 to 12 core samples under antibiotic prophylaxes and a periprostatic block. Additional core samples are needed to be taken from DRE or imaging suspicious areas (MRI or ultra-sound). There are contradictory study results about a potential superiority of MRI-targeted biopsy to ultra-sound-guided biopsy (Baco et al., 2016; Kasivisvanathan et al., 2018).

Risk Groups

Using the TNM classification, PSA level and Gleason Score PCa can be classified in three risk groups using D'Amico criteria (see Table 2): Patients are rated as low-risk patients if they

have a T stage smaller as or equal to T2a, a PSA level smaller as or equal to 10 ng/ml and a GS smaller as or equal to 6. Intermediate-risk patients show a T stage of T2b or a GS of 7 or a PSA level between 10 and 20 ng/ml. Patients are rated as high-risk patients if they have a T stage higher as or equal to T2c or a PSA level higher as or equal to 20 ng/ml or a GS higher as or equal to 8 (D'Amico et al., 1998).

Table 2: *Risk group classification of prostate carcinoma using D'Amico criteria*

	Low risk	Intermediate risk	High risk
T stage	</= T2a	T2b	>/= T2c
PSA level	</= 10ng/ml	10 – 20ng/ml	>/= 20ng/ml
GS	</= 6	7	>/= 8

Note. Using the criteria of D'Amico et al. PCa can be classified in low, intermediate and high risk with a corresponding T stage or PSA level or GS (D'Amico et al., 1998).

Staging

Dependent on the patients' risk group, age, comorbidities and preferences different staging options are recommended. The AWMF guidelines advice no further imaging staging for patients with low-risk PCa. Patients with high-risk PCa should have a magnetic resonance imaging (MRI) or Computer Tomography (CT) from the pelvis. If they suffer from bone pain, skeletal scintigraphy is recommended. Positron-Emission-Tomography (PET) hybrid imaging is only recommended in clinical trials for primary staging, which will be discussed below (AWMF online, 2019). Using MRI or CT, lymph node metastases are detected on the basis of their size, an enlarged lymph node is considered as suspicious. A meta-analysis showed that there was no difference in the performance of CT or MRI, but both being insufficient to reliably identify lymph node metastases, as the pooled sensitivity was 42% and 39% and the pooled specificity 82% and 82% for CT and MRI (Hövels et al., 2008). Briganti, Abdollah, et al. (2012) analysed the ability of CT scan to predict lymph node invasion and found an even smaller overall sensitivity of 13%. Looking only at patients with a nomogram-derived lymph node invasion risk higher than 50%, the sensitivity was still only 24% (Briganti, Abdollah, et al., 2012). This shows the necessity of more advanced diagnostic imaging modalities to

detect lymph node metastases, such as PSMA PET. In the new guidelines of 2021 this was taken under account (AWMF online, 2021).

Primary local treatment

There are different therapy options for each patient, such as active surveillance, watchful waiting, radical prostatectomy, radiation and brachytherapy. Therapy options should be discussed in a multidisciplinary team and the patients need to have all information about advantages and disadvantages of each therapy option to make an informed decision.

Active Surveillance

Active Surveillance is a therapy strategy for low-risk tumours in patients without relevant comorbidities and a life expectancy higher than 10 years. The aim is to start curative therapy not directly after diagnosis but immediately when there is a tumour progression. In this way overtreatment is avoided and patients can have the same life expectancy and quality without unnecessary treatment and treatment side effects. But it needs a well-structured follow up with DRE, PSA-level, rebiopsy and MRI and an intensive support of patients, who need to stand the distress of having a diagnosis without an active treatment (AWMF online, 2019; Mottet et al., 2017).

Watchful Waiting

Watchful waiting (WW) is a palliative treatment strategy, which can be applied to patients at all tumour stages. It is for patients with comorbidities and a life expectancy smaller than 10 years. The symptomatic treatment is delayed until tumour progression to avoid negative side effects and toxicity and it is only symptom orientated (AWMF online, 2019; Mottet et al., 2017). For a comparison of active surveillance and watchful waiting, see Table 3.

Table 3: *Definition of active surveillance and watchful waiting*

	Active surveillance	Watchful waiting
Treatment intent	Curative	Palliative
Follow-up	Predefined schedule	Patient specific
Assessment/Markers used	DRE, PSA, rebiopsy, mpMRI	Not predefined

Life expectancy	> 10 years	< 10 years
Aim	Minimise treatment-related toxicity without compromising survival	Minimise treatment-related toxicity
Comments	Only for low-risk patients	Can apply to patients at all stages

Note. To differentiate between active surveillance and watchful waiting differences in treatment intention, follow-up, assessment, life expectancy of the patient and the aim of treatment are needed to take into consideration.
DRE = digital rectal examination; PSA = prostate-specific antigen; mpMRI = multiparametric magnetic resonance imaging.
Table from Mottet et al. (2017).

Radical prostatectomy

Radical prostatectomy (RP) is a primary therapy option for patients with a localized PCa and life expectancy higher than 10 years. It shows benefits for overall survival (OS) and cancer specific survival (CSS) compared to watchful waiting (Holmberg et al., 2012; Mottet et al., 2017). The aim is a margin free resection of the prostate and preserving continence and potency, using a nerve-sparing RP. There are different surgery methods available (open, laparoscopic, robotic) with no evidence for the superiority of one surgery method over the others. Haglind et al. (2015) compared Robot-assisted laparoscopic radical prostatectomy (RALP) with open retropubic radical prostatectomy (RRP) and found comparable results with an incontinency rate about 20%, erectile dysfunction in about 70-75% of patients and frequency of positive surgical margins with approximately 20% in both groups. More important for the best possible result is therefore to recommend a hospital with a high rate of RPs and an experienced surgeon in his preferred surgery method (AWMF online, 2019; Mottet et al., 2017; Paul et al., 2008). An additional pelvic lymph node dissection (PLND) should be performed if the estimated risk of positive lymph nodes is higher than 5% (predictive model of Briganti, Larcher and colleagues (2012), including PSA, clinical state, GS of primary and secondary biopsy and percentage of positive cores, the latter representing the foremost predictor (Briganti, Larcher, et al., 2012)). Benefits of RP compared to radiation

therapy are a high local tumour control, an exact staging and a good response to chemotherapy in case of a tumour recurrence (Paul et al., 2008).

Definite Radiation therapy

Radiation therapy (RT) can be applied to patients with localized PCa of all risk groups. The recommended dose is between 74 and 80 Gy (AWMF online, 2019). There is a proven increased risk of developing a second cancer in the bladder, colorectum or rectum after RT, but with a low absolute risk ranking from 0,1 to 4,2%. Nevertheless it should be discussed especially with younger patients (Mottet et al., 2017; Wallis et al., 2016).

Brachytherapy

Low-dose rate brachytherapy, an implantation of permanent radioactive seeds into the prostate, can be used for patients with a localized low risk PCa. For high-dose rate brachytherapy a temporarily implantation of radioactive seeds should be used additional to external-beam radiation therapy (AWMF online, 2019; Mottet et al., 2017).

Positron-Emission-Tomography

Positron-Emission-Tomography (PET) is a diagnostic tool focusing on signals for molecular processes. A radioactive labelled molecule, which accumulates in the targets in question, is injected into the patient's vein before imaging. During the imaging procedure the radioactive atoms are emitting positrons, which are annihilated when they hit an electron, leading to a pair of gamma rays going in the direct opposite direction in an 180° ankle with an energy of 511keV each. In the line of response (LOR) detectors can measure coincident gamma rays and draw a conclusion about the annihilation localization. Using all detected annihilation events it is possible to reconstruct an image (Glatting, Wängler, & Wängler, 2017). For the image reconstruction some corrections are needed to receive a high image quality: A correction for randoms, dead time, scatter and attenuation. Random coincidences arise if within the time frame of coincidences two annihilations take place and from each pair of gamma ray only one part is detected, leading to a wrong LOR between the two detected parts of each pair (see Figure 3). Dead time describes the time between a photon detection and the next possible measurement of a separate event. Scattered coincidence means that

one gamma ray deviates from its initial path and therefore a wrong LOR is measured (see Figure 3). The attenuation depends on the tissue density and therefore absorption of the photon (Glatting et al., 2017; Meikle & Badawi, 2006).

Figure 3: *Types of coincidence events recorded by a PET scanner*

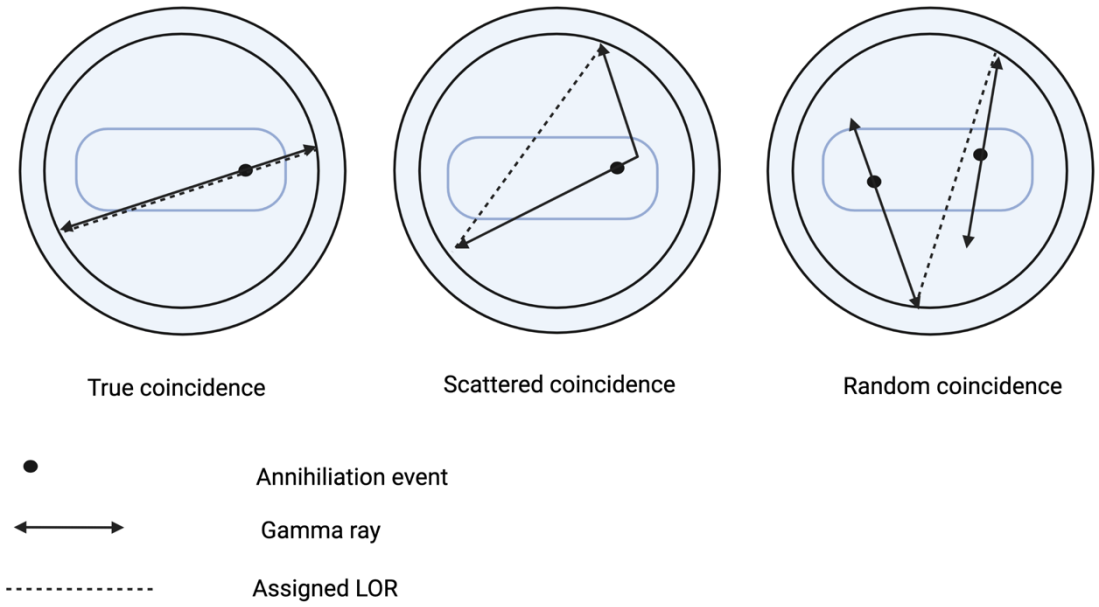

Note. A scattered coincidence happens when one gamma ray deviates from its initial path and therefore a wrong line of response (LOR) is measured.
A random coincidence arises if within the time frame of a coincidence two annihilations take place and from each pair of gamma ray only one part is detected, leading to a wrong LOR between the two detected parts of each pair.
A true coincidence takes place if with the assigned LOR the right conclusion about annihilation localization can be drawn.
Figure created with BioRender.com (n.d.), adapted from Meikle & Badawi (2006).

In the year 2000 a PET/CT hybrid scanner was introduced on the market, giving the possibility to achieve functional and anatomical information in a single scanning session as well as using CT images to correct scatter and attenuation of PET images (Beyer et al., 2000).

In 2011 a PET/MRI hybrid scanner followed, showing comparable results to the established PET/CT while giving the advantages of MRI such as increased soft tissue contrast and reduced radiation dose (Delso et al., 2011; Quick et al., 2013). Eiber et al. (2016) showed an improved diagnostic accuracy for simultaneous PET/MRI for PCa localization compared with multi parametric MRI (mpMRI) and with PET imaging alone.

Radionuclides

A radionuclide is an unstable form of a chemical element, which releases radiation as it decays (Glatting et al., 2017). ^{18}Fluorine and ^{68}Galium are two of the most used radionuclides in the imaging of prostate carcinoma. In Table 4 the two radionuclides are compared in respect to their half-life, positron energy, labelling and production.

Table 4: *Characteristics of the radionuclides ^{68}Gallium and ^{18}Fluorine*

	^{68}Galium	^{18}Fluorine
Half-life	68 minutes	110 minutes
Energy of the positron	1,90 MeV	0,65 MeV
Labelling	Chelator	Prosthetic group
Production	Generator	Cyclotron

Note. The characteristics of ^{68}Ga and ^{18}F in comparison with regard to half-life, energy of the positron, labelling and production.
Table adapted from Conti and Eriksson (2016) and Spohn et al. (2019)

Due to those differences ^{18}Fluorine offers some advantages: The lower energy of positrons leads theoretically to a higher image resolution and a lower radiation exposure. The production in a cyclotron and the longer half-life leads to an easier way of production and distribution. It is possible to produce in large scale and supply other hospitals (Conti & Eriksson, 2016; Spohn et al., 2019). Using the Monte Carlo Simulation in different tissues studies could show a higher image resolution for radionuclides with a lower positron emission, such as ^{18}Fluorine (Cal-González et al., 2009; Levin & Hoffman, 1999; Sánchez-Crespo, Andreo, & Larsson, 2004). The lower image resolution is especially seen in high resolution PET scanners (De Jong et al., 2005; Disselhorst et al., 2010), whereas in present

commercial PET scanners the difference might not be measurable (Conti & Eriksson, 2016; Soderlund et al., 2015). To some point the lower spatial resolution can be compensated with mathematical corrections (Cal-González et al., 2009; Derenzo, 1986; Kotasidis et al., 2014). A cyclotron is a particle accelerator, which is used since the 1930s to produce short-lived positron-emitting radionuclides. ^{18}Fluorine is produced by the reaction of an accelerated proton (p) with ^{18}oxygen, generating a neutron (n) and ^{18}Fluorine in a so called ^{18}O(p,n)^{18}F reaction (Glatting et al., 2017; Mason & Mathis, 2005).

Targets

Increased metabolism and proliferation

As tumour tissue shows an increased glucose metabolism and proliferation it is possible to visualize the accumulation of Fluorodeoxyglucose (FDG) or Choline, which is needed for the synthesis of cell membranes. ^{18}F-FDG is the most common used tracer in oncology due to the increased need of energy and therefore increased glucose metabolism in malignant tissue compared to normal tissue (Glatting et al., 2017). But as most PCas are slowly-growing and show only a low glycolytic rate ^{18}F-FDG does not play an important role in the imaging of PCa (Jadvar, 2013; Liu, Zafar, Lai, Segall, & Terris, 2001). There was some hope that choline derivatives will achieve better results (Eiber et al., 2017; Glatting et al., 2017) and the U.S. Food and Drug Administration (FDA) approved ^{11}C-choline for imaging biochemical recurrent prostate cancer in 2012 (U.S. Food and Drug Administration, 2012). But a meta-analysis of 2013 showed that ^{18}F- and ^{11}C-choline PET can only show a high specificity (the pooled specificity was 95%), but no high sensitivity (the pooled sensitivity was 49.2%) (Evangelista, Guttilla, Zattoni, Muzzio, & Zattoni, 2013). In contrast to this a meta-analysis published six years later by Lin, Lee, Lin, and Kao (2019) showed a high performance of ^{18}F-Choline PET/CT with a pooled sensitivity and specificity of 93% (95% CI, 0.91–0.94) and 83% (95% CI, 0.80–0.85). Another target is the upregulation of amino acid transportation in prostate cancer cells. Due to this upregulation ^{18}F-fluciclovine (anti-1-amino-3–18 F-fluorocy-clobutane-1-carboxylic acid [FACBC]) which is a radiolabeled amino acid analog shows an increased uptake in prostate cancer cells (Gusman et al., 2019). In a direct comparison of the lesion detection rate of ^{11}C-choline versus ^{18}F-fluciclovine PET/CT in patients with increasing PSA levels after radical treatment of prostate cancer, ^{18}F-fluciclovine showed a better performance with a sensitivity of 37% versus 32% (Nanni et al.,

2015, 2016). In 2016 it was approved by the FDA for recurrent prostate cancer (Axumin®) (U.S. Food and Drug Administration, 2016).

PSMA – prostate specific membrane antigen

Prostate specific membrane antigen (PSMA) is a transmembrane glycoprotein with enzymatic activity and an excellent target in PCa for multiple reasons: It is significantly overexpressed on almost all PCa cells and in advanced stages the expression is further increased (Bostwick, Pacelli, Blute, Roche, & Murphy, 1998; Silver, Pellicer, Fair, Heston, & Cordon-Cardo, 1997). After the binding of ligands to the active centre of the extracellular domain of PSMA they are internalized. On the basis of endosomal recycling, it leads to a higher tumour uptake and retention and therefore high image quality (Ghosh & Heston, 2004; Rajasekaran et al., 2003; Schwarzenboeck et al., 2017). A further advantage is the PSA independent regulation of PSMA expression (Bostwick et al., 1998). Another interesting characteristic of PSMA is the expression in neovasculature of other solid tumours (e.g. bladder, gastric and colorectal cancer), which involves potential pitfalls in imaging especially in PCa invading the bladder but also the chance for theranostic applications in other solid tumours (Chang et al., 1999; Haffner et al., 2009; Samplaski, Heston, Elson, Magi-Galluzzi, & Hansel, 2011). Furthermore it is expressed on astrocytes in the central nervous system, there it is called glutamate carboxypeptidase 2 (Carter, Feldman, & Coyle, 1996; Maurer, Eiber, Schwaiger, & Gschwend, 2016).

PSMA targeting agents

Due to the above mentioned advantages of PSMA there has been a lot of research about PSMA targeting agents such as antibodies and small-molecule PSMA ligands. Okarvi (2019) for example was recently giving a good overview about this topic.

Anti-PSMA antibodies

So far ^{111}Indium capromab pendetide (ProstaScint®) was approved by the FDA in 1996 (Zuckier & DeNardo, 1997): it is a radiolabelled anti-PSMA antibody targeting an intracellular epitope (7E11) of PSMA as can be seen in **Figure *4***. Because the intracellular site is not detectable for circulating antibodies capromab is especially weak in detecting bone

metastases. As bone metastases occur in approximately 75% of patients, the clinical utility of capromab is considerably compromised (Bander, 2006). Additionally antibodies show a low diagnostic effectiveness because of their long blood circulation and therefore a high unspecific background activity as well as low tumour penetrability (Maurer, Eiber, et al., 2016).

Figure 4: *PSMA binding sites*

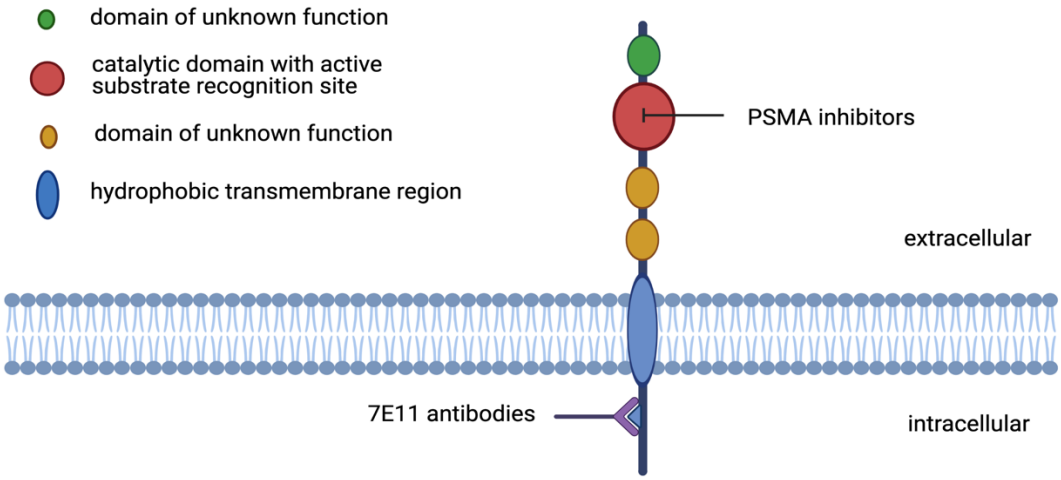

Note. The structure of the prostate specific membrane antigen (PSMA) with its binding sites for PSMA inhibitors and 7E11 antibodies. 7E11 antibodies are binding to the intracellular domain. The blue part is representing the hydrophobic transmembrane region. The extracellular domain consists of two domains of unknown function, represented in yellow, with proline- and glycine-rich domains as linkers. The red part is embodying the catalytic domain with the active substrate recognition site, which PSMA inhibitors are targeting. The green part is another domain with so far, no known function.
Figure created with BioRender.com (n.d.), adapted from Maurer, Eiber, et al. (2016).

Small-molecule PSMA ligands/inhibitors

The development of small-molecule PSMA ligands (i.e. peptides, peptidomimetics) was promoted by the discovery of structural and functional homology of the active substrate of PSMA and the glutamate carboxypeptidase 2 (also known as N-acetylated-α-linked acidic dipeptidase I) (Maurer, Eiber, et al., 2016; Mesters et al., 2006; Tiffany, Lapidus, Merion, Calvin, & Slusher, 1999). There are two pockets in the recognition site of PSMA: a glutamate-sensing pocket (S1`) and the non-pharmacophore pocket (S1), and two zinc ions. Most inhibitors contain a zinc-binding component and glutamate or glutamate isostere, which resides in the S1` pocket (Maurer, Eiber, et al., 2016). From the three groups of PSMA ligands (phosphorous-based, thiol-based and urea-based) the urea-based ligands present the clinically most advanced group. As shown in **Figure *5*** they contain three components: a target-binding motif (binding PSMA), a radiolabel-binding moiety, which can be a chelator molecule (for ^{68}Ga) or a prosthetic group (for ^{18}F), and a linker between the binding motif and radiolabel-binding moiety (Eiber et al., 2017). The binding motif Glutamate-Urea-Lysin (Glu-urea-Lys) is the currently preferred scaffold (Eiber et al., 2017). Another possible motif is Glutamate-Urea-Glutamate (Glu-urea-Glu) (Okarvi, 2019). Recently the most widely used PSMA ligands are ^{68}Gallium or ^{18}Fluorine labelled. In ^{68}Ga-labeled PSMA ligands ^{68}Ga-PSMA-11 (^{68}Ga-PSMA-HBED-CC) and the theranostic agents ^{68}Ga-PSMA-617 and ^{68}Ga-PSMA-I&T are of high interest (Eiber et al., 2017). Theranostic agents include the possibility of both diagnosis and therapy as the PSMA ligand can be labelled with ^{68}Ga for imaging, ^{111}In for radioguided surgery and ^{177}Lu for therapy (Maurer, Eiber, et al., 2016).

In 2020 ^{68}Ga-PSMA-11 was the first PSMA-targeting PET imaging drug which was approved by the FDA (U.S. Food and Drug Administration, 2020).

^{18}F-DCFBC, ^{18}F-DCFPyL, and ^{18}F-PSMA 1007 are the most widely used ^{18}F-labeled PSMA ligands (Eiber et al., 2017). ^{18}F-DCFPyL, also named Piflufolastat F 18, was the second PSMA-targeting PET imaging drug approved by the FDA (Pylarify®) (Keam, 2021; U.S. Food and Drug Administration, 2021).

^{18}F-labeled PSMA ligands show the mentioned advantages compared to ^{68}Ga-labeled PSMA ligands: cyclotron production of ^{18}F offers a higher amount of ^{18}F available and therefore an increased number of possible examinations. Furthermore, the longer half-life allows an easier distribution to other clinics. Another advantage lies in the lower positron energy of ^{18}F, facilitating a better image quality (Maurer, Eiber, et al., 2016).

Figure 5: *Structural components of urea-based PSMA ligands*

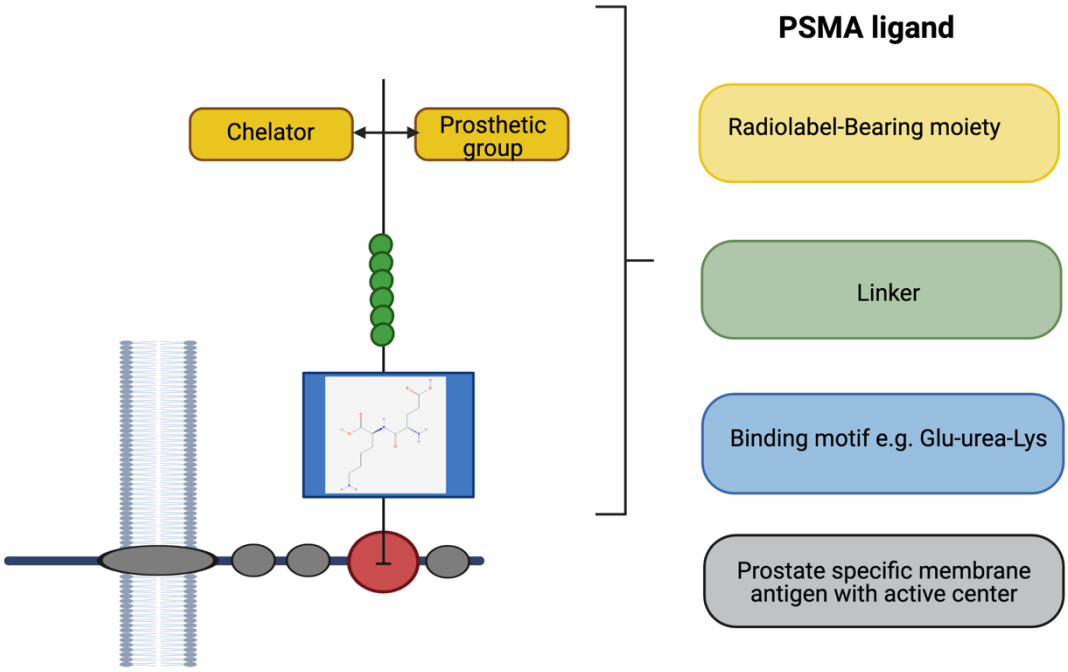

Note. Urea-based PSMA ligands contain three components: a target-binding motif, shown in blue, binding itself to the active centre of PSMA, which is shown in red; a radiolabel-binding moiety (represented in yellow) which can be a chelator molecule (for ^{68}Ga) or a prosthetic group (for ^{18}F), and a linker between the binding motif and radiolabel-binding moiety, shown in green.

Figure created with BioRender.com (2021), adapted from Eiber et al. (2017), chemical structure for Glu-urea-Lys from the National Center for Biotechnology Information (2021).

rhPSMA – radiohybrid PSMA

In 2019 a new class of ^{18}F-labeled PSMA ligands was introduced: radiohybrid PSMA (rhPSMA) ligands which are also agents with theranostic qualities as they can be labelled with ^{18}Fluorine and radiometals such as ^{68}Gallium or ^{177}Lutetium (Wurzer, Di Carlo, et al., 2020). Wurzer, Di Carlo et al. (2020) used a Silicon-Fluoride-Acceptor (SiFA) moiety which can be labelled by isotopic exchange (^{19}F → ^{18}F). Because SiFA units have a low lipophilicity (Höhne et al., 2008), they added a chelator to the same molecule, which can either complex a cold

(non-radioactive) metal (e.g. ^{nat}Ga or ^{nat}Lu) or can be labelled with a radiometal (e.g. ^{68}Ga or ^{177}Lu), while the SiFa moiety is non-radioactive (^{19}F) (Wurzer, Di Carlo, et al., 2020). With this technique they developed the chemical identical twins ^{18}F-^{nat}Ga-rhPSMA and ^{68}Ga-^{19}F-rhPSMA, which offer the possibility that biochemical findings with one ligand can be transferred to its twin (see Figure 6, A). Furthermore the possible use of ^{18}F-^{nat}Lu-rhPSMA and ^{19}F-^{177}Lu-rhPSMA might build a bridge between diagnostics and therapy, as pretherapeutic imaging and dosimetry as well as therapy could be conducted with the same tracer (Wurzer, Di Carlo, et al., 2020) (see Figure 6).

The lead compound of this class, ^{18}F-rh-PSMA-7, which is a Glu-Urea-Glu (Glutamin-Urea-Glutamin) based ligand, shows a comparable biodistribution to established PSMA ligands. It has a low accumulation in the bladder, clearly lower than ^{68}Ga-PSMA-11, which leads to better conditions to evaluate this region. Tumour uptake is comparable to ^{68}Ga-PSMA-11 and the uptake in background tissue is low (Oh et al., 2019). Regarding binding affinities and internalization rates ^{18}F-rhPSMA-7 shows similar or better results than ^{18}F-DCFPyL and ^{18}F-PSMA-1007 (Wurzer, Di Carlo, et al., 2020), see Figure 7.

Figure 6: *Radiohybrid prostate specific membrane antigen - rhPSMA*

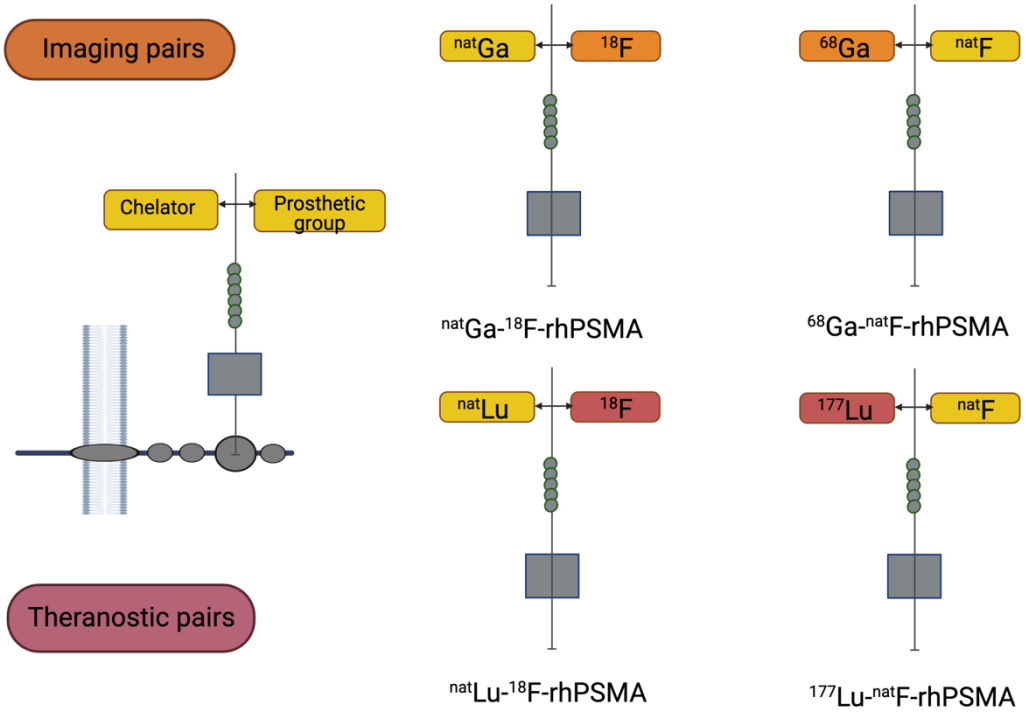

Note. Examples of radiohybrid PSMA-inhibitors: one of the binding sites is "labelled" with a radioisotope (^{68}Ga, ^{177}Lu, ^{18}F), the other one is silent, thus "labelled" with a nonradioactive isotope (^{nat}Ga, ^{nat}Lu, ^{nat}F). These pairs of compounds, either pure imaging pairs or theranostic pairs represent chemically identical twins and thus exhibit identical in vivo characteristics (affinity, lipophilicity, pharmacokinetics etc.). ^{68}Ga and ^{177}Lu are examples that can be substituted by other (radio-)metals.

Figure created with BioRender.com (2021), adapted from Wurzer, Di Carlo, et al. (2020).

Figure 7: *Binding affinities and internalized activity of radiohybrid prostate specific antigen (rhPSMA)*

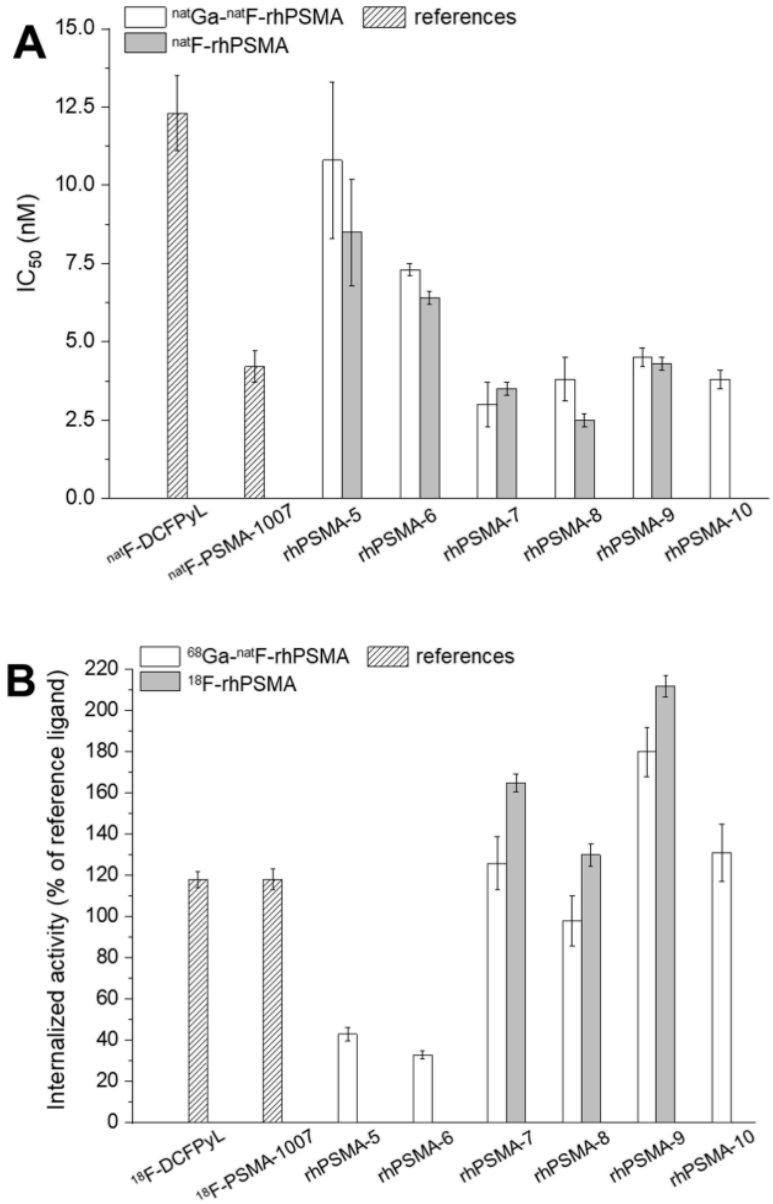

Note. A) Binding affinities (IC50 in nM, 1 h, 4°C; n=3) of ^{nat}Ga-^{nat}F-rhPSMA-5–10 (white bars), ^{nat}F-rhPSMA-5–10 with free chelator (grey bars) and ^{nat}F-DCFPyL and ^{nat}F-PSMA-1007 (as reference in striped bars).

IC50 stands for the half maximal inhibitory concentration, the IC50 value reflects the concentration of a ligand that is needed to reduce the binding of another ligand to 50%.

B) Internalized activity of ^{18}F-DCFPyL and ^{18}F-PSMA-1007 (as reference in striped bars), ^{68}Ga-^{nat}F-rhPSMA-5–10 (white bars) and ^{18}F-rhPSMA-5–10 with free chelator (grey bars), in LNCaP cells (1 h, 37°C) as percent of the reference ligand (125I-I-BA)KuE; n=3).

LNCaP (lymph node carcinoma of the prostate) is a cell line originating from a metastatic lesion of human prostatic adenocarcinoma, which grows readily in vitro (Horoszewicz et al., 1983) which is used in research about prostate cancer.

Figure and explanation from Wurzer, Di Carlo, et al. (2020). This research was originally published in the Journal of Nuclear Medicine: Wurzer, A., Di Carlo, D., Schmidt, A., Beck, R., Eiber, M., Schwaiger, M., & Wester, H. J. (2020). Radiohybrid ligands: A novel tracer concept exemplified by 18F- or 68Ga-labeled rhPSMA inhibitors. *Journal of Nuclear Medicine*, *61*, 735–742.

Rh-PSMA: Latest developments

For this study a diastereomeric mixture has been used. ^{18}F-rhPSMA-7 was composed of four stereoisomers (^{18}F- ^{nat}Ga-rhPSMA-7.1, -7.2, -7.3 and -7.4), differing in the stereoconfiguration of diaminopropionic acid (D-/L-Dap) and DOTA-GA (R-/S-DOTA-GA). The stereoisomer 7.1 contains a D-Dap and R-DOTA-GA, stereoisomer 7.2 a L-Dap and R-DOTA-GA, stereoisomer 7.3 a D-Dap and S-DOTA-GA and stereoisomer 7.4 a L-Dap and S-DOTA-GA (Wurzer, Parzinger, et al., 2020). After ^{18}F-rhPSMA-7 has been successfully assessed in clinical studies the most promising stereoisomer of the diastereomeric mixture has been identified. ^{18}F-rhPSMA-7.3 showed a lower enrichment in blood, liver and kidney but also displayed a high tumour uptake. In addition, ^{18}F-rhPSMA-7.3 represented 40% of the diastereomeric mixture. Therefore it typifies the most favourable stereoisomer to be used in further clinical research (Wurzer, Parzinger, et al., 2020). Yusufi et al. (2021) examined the preclinical biodistribution, dosimetry and therapeutic efficacy of ^{19}F-^{177}Lu-rhPSMA-7.3 in comparison to the established therapeutic agent ^{177}Lu-PSMA I&T (imaging & therapy). The new tracer ^{19}F-^{177}Lu-rhPSMA-7.3 showed a superior tumour uptake and retention, while

having similar clearance kinetics and radiation dose to healthy organs compared to ^{177}Lu-PSMA I&T. Wurzer et al. (2021) developed a fast and reliable automated production of ^{18}F-rhPSMA-7 and ^{18}F-^{nat}Ga-rhPSMA-7.3 which increase the chances of a successful clinical translation. The radiohybrid agent can thereby be produced within 16 minutes with a reliability of 98.8%.

For the evaluation of the suitability of ^{18}F-rhPSMA-7 for clinical imaging Tolvanen et al. (2020) studied the safety, biodistribution and radiation dosimetry of the new tracer in 6 healthy adults (three men and three women). They found the tracer to be well tolerated by the subjects, with a mean effective dose of 0.0141 mSv/MBq and the adrenals, kidneys and salivary glands as the organs with the highest absorbed dose per unit of administered radioactivity. The urine excretion of the injected radioactivity was about 7%.

Diagnostic accuracy of PSMA ligands for primary staging

^{68}Ga-PSMA-11

For the evaluation of the diagnostic accuracy of ^{68}Ga-PSMA-11 as a reference for the ^{18}F-rh-PSMA-7 under study it needs a look at meta-analysis about this topic.

A meta-analysis of Perera et al. (2019) reported a summary sensitivity of five studies of ^{68}Ga-PSMA-11 PET of 75% [0.58–0.87] and a summary specificity of 99% [0.97–1.00] on a per-lesion analysis and a summary sensitivity of 77% [0.46–0.93] and specificity of 97% [0.91–0.99] on a per-patient analysis for primary staging with histology-proven disease.

The meta-analysis of Hope et al. (2019) comes to a comparable result with a sensitivity of 74% (95% CI, 0.51–0.89) and specificity of 96% (95% CI, 0.85–0.99), analysing six studies with histopathology as gold standard. Four studies were analysed in both meta-analyses.

One of those was the study of Maurer, Gschwend, et al. (2016), who analysed the diagnostic accuracy of ^{68}Ga-PSMA-11-PET in comparison to morphological imaging for 130 patients. They reported a patient-based sensitivity, specificity and accuracy of ^{68}Ga-PSMA-11-PET of 65.9% (95% CI, 49.4–79.9), 98.9% (95% CI, 93.9–100) and 88.5% (95% CI, 81.7–93.4). Whereas those of morphological imaging were 43.9%, 85.4% and 72.3%, respectively.

The template-based analysis led to a sensitivity, specificity and accuracy of ^{68}Ga-PSMA-PET of 68.3%, 99.1% and 95.2%, and the analysis of morphological imaging showed a sensitivity, specificity and accuracy of 27.3%, 97.1% and 87.6% (Maurer, Gschwend, et al., 2016).

Except for van Leeuwen et al. (2017) the study design was retrospective.

These results lead to the conclusion, that ^{68}Ga-PSMA-11 PET is superior to morphological imaging in the detection of lymph node metastases, but also that there is still more need of prospective high quality study designs, using histopathology as validation (Corfield, Perera, Bolton, & Lawrentschuk, 2018; Esen, Kılıç, Seymen, Acar, & Demirkol, 2020). For the detection of skeleton lesions ^{68}Ga-PSMA-PET/CT also showed significantly higher sensitivity and accuracy than bone scintigraphy (96.2% vs. 73.1%, and 99.1% vs. 84.1%) (Lengana et al., 2018). In 2020 Hofman and colleagues published the results of a prospective randomized study which analyzed the diagnostic accuracy of CT and skeletal scintigraphy in comparison with ^{68}Ga-PSMA-11 PET/CT. ^{68}Ga-PSMA-11 PET/CT showed superior results with an accuracy of 92% [88–95] compared to 65% [60–69] of conventional imaging. They found a higher sensitivity (85% [74–96] vs. 38% [24–52]) and specificity (98% [95–100] vs. 91% [85–97]) for ^{68}Ga-PSMA PET-CT compared with conventional imaging (Hofman et al., 2020).

^{18}F-PSMA ligands

As the research about ^{18}F-PSMA ligands is relatively new there is only a small number of studies available about the diagnostic efficacy in primary staging. Giesel et al. (2017) compared the results of ^{18}F-PSMA-1007 PET/CT and histopathology of eight patients after RP and PLND. In total 309 pelvic lymph nodes were dissected, 19 showing metastases. ^{18}F-PSMA-1007 PET/CT detected 18 of 19 lymph node metastases with a sensitivity of 94.7%. As there was no false positive finding in the patient cohort the specificity was 100%. Bodar et al. (2019) evaluated twenty patients and found a sensitivity of 63% and a specificity of 95% of ^{18}F-PSMA-DCFPyL -PET/CT. The performance of ^{18}F-PSMA-DCFPyL-PET was also evaluated by Gorin et al. (2018) who reported a sensitivity of 71.4% (95% CI, 29.0–96.3) and specificity of 88.9% (95% CI, 65.3–98.6) on a patient based analysis of twenty-five patients. The sensitivity and specificity on the level of individual nodal packets were 66.7% (95% CI, 29.9–92.5) and 92.7% (95% CI, 80.1–98.5), respectively.

Kesch et al. (2017) compared ^{18}F-PSMA-1007 PET/CT with mpMRI in ten patients, achieving a sensitivity of 71% and specificity of 81% for ^{18}F-PSMA-1007 PET/CT and a sensitivity of 86% and specificity of 64% for mpMRI. Giesel et al. (2018) showed a comparable diagnostic efficacy of ^{18}F-PSMA-1007 and ^{18}F-PSMA-DCFPyl with both having an excellent imaging quality. Kuten et al. (2019) presented comparable results for the diagnostic efficacy of ^{18}F-PSMA-1007 and ^{68}Ga-PSMA-11 in the detection of intra-prostatic lesions for sixteen patients

who underwent imaging with both radiotracers within fifteen days. According to Rautio, Kivi, Poksi and Šamarina (2019) ^{18}F-PSMA 1007 shows a significantly better sensitivity and specificity than 99mTc-bone scan in detecting bone metastases.

In summary it can be said, that ^{18}F-PSMA ligands show promising results and ^{18}F-rhPSMA-7 offers especially favourable characteristics such as high batch production, low urinary accumulation and the option to be used for diagnostic and therapy due to the radiohybrid concept. But there are only few studies with high patient numbers and histopathological confirmation.

This study compares the diagnostic efficacy of ^{18}F-rhPSMA-7 PET with morphological imaging and is validated by histopathology for the primary staging of fifty-eight patients with intermediate or high-risk prostate carcinoma. A comparison with literature about the diagnostic efficacy of ^{68}Ga-PSMA 11 is also made.
Systematic literature search for the theoretical background took place in March 2020.

Methods

Patients

During the time period of one year (July 2017 until June 2018) all patients who underwent radical prostatectomy and extended pelvic lymph node dissection after primary staging with ^{18}F-rhPSMA-7 PET/CT or PET/MRI at the Klinikum rechts der Isar, Munich, were retrospectively included in a database. All patients signed a written informed consent for the anonymized evaluation and publication of their data. Patient information was retrospectively received from SAP (Walldorf, Germany) of the department of Nuclear Medicine, the department of Urology and the department of Radiotherapy as well as from PACS (Picture Archiving and Communication System) of the department of Nuclear Medicine. Collected data included: Prostate carcinoma correlated data (among others: first diagnosis, initial and following PSA-Score, GS of biopsy, initial therapy), data about the ^{18}F-rhPSMA-7 PET/CT or PET/MRI examination (among others: patients' weight, injected activity in MBq, uptake time) and follow-up information of each registered patient over the time period of 12 month (further treatment, PSA-Score, histology from RP). Included in further

analysis were patients with a histologically proven PCa who underwent RP with extended PLND at the Klinikum rechts der Isar and who did not receive any neoadjuvant treatment before or after primary staging. In total fifty-eight patients were included in the data analysis (for a flowchart of patient selection see Figure 8). The analysis got an approval by the local Ethics Committee (permit 290/18S). Administration of ^{18}F- rhPSMA-7 complied with the German Medicinal Products Act, AMG x13 2b, and the responsible regulatory body (government of Oberbayern).

Figure 8: *Flow chart of patient selection*

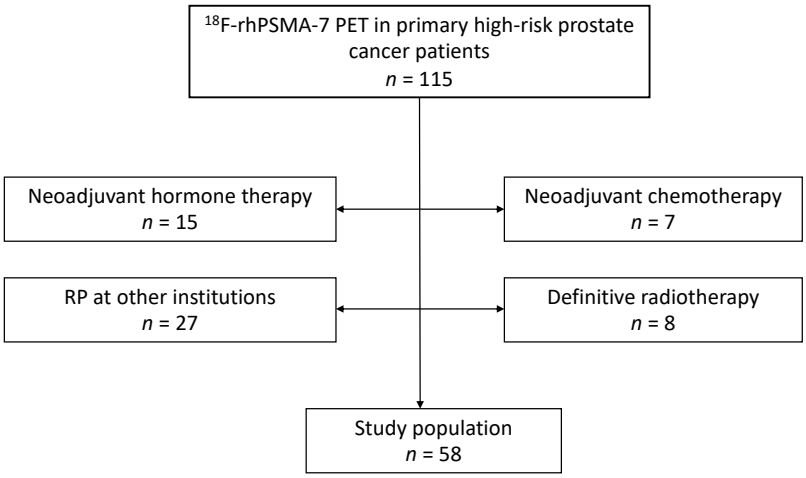

Note. 115 patients with a high-risk prostate carcinoma who underwent radical prostatectomy (RP) within 12 months were retrospectively included in a database. Due to adjuvant therapy (hormone or chemotherapy) 22 patients were excluded from further analysis. Another 27 patient underwent RP at other institutions and were therefore excluded in order to guarantee the same surgery standards and access to follow up information for all patients. Eight patients had a definitive radiotherapy instead RP and were therefore excluded, which lead to a study population of 58 patients.

^{18}F-rhPSMA-7 Synthesis and PET imaging

The diagnostic ^{18}F-rhPSMA-7 technology has been developed at the Technical University of Munich. A detailed description of ^{18}F-rhPSMA-7 synthesis can be received from Wurzer, Di Carlo, et al. (2020).

^{18}F- rhPSMA-7 was administered as an intravenous bolus before scanning. The PET/CT and PET/ MRI acquisitions were executed as described previously by Eiber et al. (2015) and Souvatzoglou et al. (2013). All patients received diluted oral contrast medium (300 mg of ioxitalamate [Telebrix; Guerbet]) and the diuretic Furosemid (20mg). All PET scans were acquired in 3-dimensional mode with an acquisition time of two minutes per bed position in flow technique (equals 1.1 mm/s) for PET/CT and four minutes per bed position for PET/MRI. Emission data was corrected for randoms, dead time, scatter, and attenuation and was reconstructed iteratively by an ordered-subsets expectation maximization algorithm (four iterations, eight subsets) followed by a postreconstruction smoothing gaussian filter (5mm in full width at half maximum).

Image analysis

Two experienced physicians, one board-certified radiologist and nuclear medicine specialist and one board-certified nuclear medicine specialist were reviewing all ^{18}F-rhPSMA-7 PET/CT and PET/MRI datasets. They were blinded to the RP and PLND histology results. The image analysis took place in a two-step procedure. First anatomic data from CT (diagnostic contrast-enhanced CT) and MRI (pelvic axial T2-weighted turbo spin-echo and the whole-body axial T2-weighted half-Fourier single-shot turbo spin-echo) were analysed. After at least four weeks a second reading, this time of ^{18}F-rhPSMA-7 PET scans was performed. Analysing the PET/CT and PET/MRI scans morphological information was only used for anatomic allocation. A focus of increased uptake could so be assigned to the corresponding lymph node template. In both steps each lymph node template in PET and in CT or MRI was rated using a 5-point Likert scale reaching from 1 – tumour manifestation to 5 – benign. For PET the following criteria were used: an intense, focal ^{18}F-rhPSMA-7 uptake, higher than uptake in the liver was rated as 1 – tumour manifestation. An ^{18}F-rhPSMA-7 uptake clearly higher than the background level in vessels but not higher than in the liver was rated as 2 – probable tumour manifestation. An ^{18}F-rhPSMA-7 faint uptake between the background level in muscle tissue and the background level in vessels was rated as 3 – equivocal. An ^{18}F-

rhPSMA-7 uptake as faint as the background level, e.g., equal to the level in adjacent muscle was rated as 4 – probable benign and no ^{18}F-rhPSMA-7 uptake was rated as 5 – benign. For CT and MRI, the following criteria were used: A short-axis diameter > 10mm was rated as 1 – tumour manifestation. A short-axis diameter of 8–10mm, a round configuration, and a regional grouping was rated as 2 – probable tumour manifestation. A short-axis diameter of 8–10mm, an oval configuration, and no regional grouping was rated as 3 – equivocal. A short-axis diameter < 8mm was rated as 4 – probable benign and a short-axis diameter < 5mm was rated as 5 – benign.

Histopathology

During RP, extended PLND was performed as previously described from Heck et al. (2014). The standard lymph node templates which are used in the Department of Urology and were collected separately are the following: right/left common iliac vessel, right/left internal iliac vessel, right/left external iliac vessel, and right/ left obturator fossa as can be seen in Figure 9. When preoperative imaging showed ^{18}F-rhPSMA- 7 PET–positive lymph nodes outside these regions, additional templates (e.g. presacral/pararectal) were resected. Since exact lymph node tracking is impossible, especially normal-sized lymph nodes, a template-based analysis of resected lymph nodes was chosen. Tissue from each template was sent separately for histological evaluation. The uropathologists were blinded to the preoperative imaging results.

Figure 9: *Templates for extended pelvic lymph node dissection*

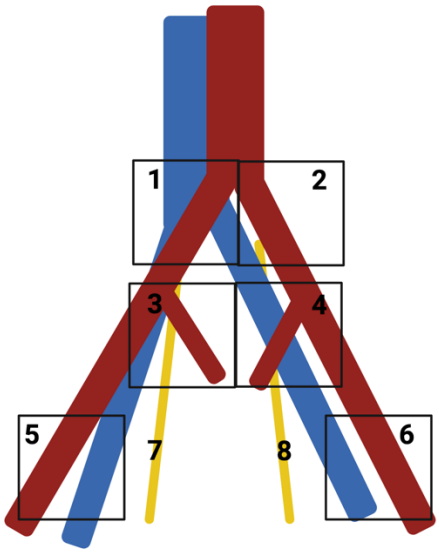

Note. Extended pelvic lymph node dissection included bilateral dissection of the right and left common iliac vessels (area 1 and 2), the right and left internal iliac vessels (area 3 and 4), the right and left external iliac vessels (area 5 and 6), and the right and left obturator fossa (area 7 and 8)

Figure created with (BioRender.com, 2021), adapted from Heck et al. (2014).

Statistical Analysis

The histopathologic results from resected lymph nodes were brought into relation with the results of morphological imaging (MRI or CT) and ^{18}F-rhPSMA-7 PET in a patient- and template-based manner. The overall diagnostic accuracy of patient-level data was assessed using receiver-operating-characteristic (ROC) analyses for both, ^{18}F-rhPSMA-7 PET and morphological imaging. Areas under the ROC curves (AUCs) with 95% confidence intervals (CIs) were calculated and compared with each other. For patient-based analysis, the method of DeLong et al. (DeLong, DeLong, & Clarke-Pearson, 1988) was used, and the approach of Obuchowski (1997) was applied for template-based analyses to account for correlations of multiple assessments within one patient. The semiquantitative 5-point-Likert-Scale was dichotomized to estimate sensitivities, specificities and accuracies. For the dichotomization the Youden index (sensitivity + specificity - 1) was used to determine the best cut-off.

In the patient-based analyses, exact CIs were estimated for these measures on the basis of the binomial distribution (Clopper–Pearson intervals, (Clopper & Pearson, 1934)). For the template-based analyses, logistical generalized-estimating-equation (GEE) models were fitted to the data to account for the correlation of multiple observations within the same patient (Smith & Hadgu, 1992; Zeger & Liang, 1986). For estimation of sensitivities with associated CIs, only templates with a positive histologic result were included, and the result of the diagnostic test was used as a dependent variable. To derive estimates for the specificities, a variable indicating whether a negative test result was observed was used as a dependent variable, and only patients with a negative histopathologic result were included. Accuracy was estimated in an intercept-only model with a dependent variable that indicated whether the test result and the result of the histopathologic assessment agreed. For the GEE model, an independent correlation structure was assumed. A significance level of 5% was considered for all tests. All statistical analyses were performed using the statistical software R (R Core Team, 2020), with its packages pROC (Robin et al., 2011) and geepack (Halekoh, Højsgaard, & Yan, 2006).

Results

Patients' characteristics

All patients suffered from a high-risk PCa, defined by D'Amico et al. (1998), that means all patients had an initial PSA score higher or equal to 20 ng/ml or a Gleason Score higher or equal to 8 or a clinical T staging higher or equal to 2c (D'Amico et al., 1998). ^{18}F- rhPSMA-7 was administered as an intravenous bolus with a median activity of 328 MBq (range 132–410 MBq) and a median of 82 minutes (range 60–153 min) before scanning. Thirty-nine patients underwent contrast- enhanced ^{18}F-rhPSMA-7 PET/CT (Biograph mCT Flow; Siemens Medical Solutions). Nineteen patients underwent ^{18}F-rhPSMA-7 PET/MRI (Biograph mMR; Siemens Medical Solutions).

Further patients' characteristics are presented in Table 5.

Table 5: *Patients' characteristics*

Characteristics	
Total	
N	58
Age, (y)	
Mean	67.7
Median	68
IQR	65–73
Range	48–80
PSA at imaging, ng/ml	
Mean	18.1
Median	12.2
IQR	7.3–22.4
Range	1.2–81.6
Gleason Score, n	
7a	11 (19.0%)
7b	25 (43.1%)
8	4 (6.9%)
9	18 (31.0%)
10	0
Pathological T-stage, n	
≤ pT2c	26 (44.8%)
pT3a	12 (20.7%)
≥ pT3b	20 (34.5%)
Pathological N-stage	
pN0	40 (69%)
pN1	18 (31%)
Lymph nodes removed (n)	
Total	1137
Median	18
IQR	8

Range	8–53
Lymph nodes with metastasis (n)	
Total	71
Median	0
IQR	1
Range	0–15
Injected activity (MBq)	
Mean	327.7
Median	327
IQR	306.5–363
Range	132–410
Uptake time (min)	
Mean	82
Median	79.5
IQR	70–87.25
Range	60–153

Note. Description of patients' characteristics, including age, PSA score at imaging, Gleason Score, T and N stage, Lymph nodes removed, lymph nodes with metastasis, injected activity and uptake time.

IQR = interquartile range

Histopathological results and ROC analysis

In 18 of the 58 patients (31.0%) lymph node metastases were found in histopathology. In total 375 lymph node templates were resected, 52 showed metastases (13.9%). A local tumour was detected in 57 patients (98,3%) by ^{18}F-rhPSMA-7 PET, whereby one patient was showing evidence of distant lymph node and bone metastases (1,9%).

For morphological imaging, a score of 1, 2, or 3 on the Likert scale was regarded as positive, whereas a score of 4 or 5 was considered negative, on the basis of the Youden index (the Youden Index on patient-based analysis was 0.197 for 1-2 vs. 3-5 and 0.225 for 1-3 vs. 4-5; on template-based analysis the Youden Index was 0.007 for 1-2 vs. 3-5 and 0.046 for 1-3 vs. 4-5).

For ^{18}F-rhPSMA-7 PET, a score of 1 or 2 was considered positive, whereas a score of 3, 4, or 5 was regarded as negative (the Youden Index on patient-based analysis was 0.647 for 1-2 vs. 3-5 and 0.578 for 1-3 vs. 4-5; on template-based analysis the Youden Index was 0.507 for 1-2 vs. 3-5 and 0.496 for 1-3 vs. 4-5).

On patient-based analysis for the detection of lymph node metastases, ROC curves showed an AUC of 0.858 (95% CI, 0.739–0.978) for ^{18}F-rhPSMA-7 PET and 0.649 (95% CI, 0.492–0.805) for morphologic imaging, see Figure 11, A.

On template-based analysis, ROC curves showed an AUC of 0.766 (95% CI, 0.697–0.834) for ^{18}F-rhPSMA-7 PET and 0.589 (95% CI, 0.522–0.656) for morphologic imaging alone, see Figure 11, B.

^{18}F-rhPSMA-7 PET performed significantly better than morphologic imaging alone on patient-based analysis (difference in AUCs = 0.210; 95% CI, 0.046–0.373; $p = 0.012$) and template-based analysis (difference in AUCs = 0.177; 95% CI, 0.104–0.249; $p < 0.001$).

A representative sample can be seen in Figure 10.

Figure 10*: Patient example*

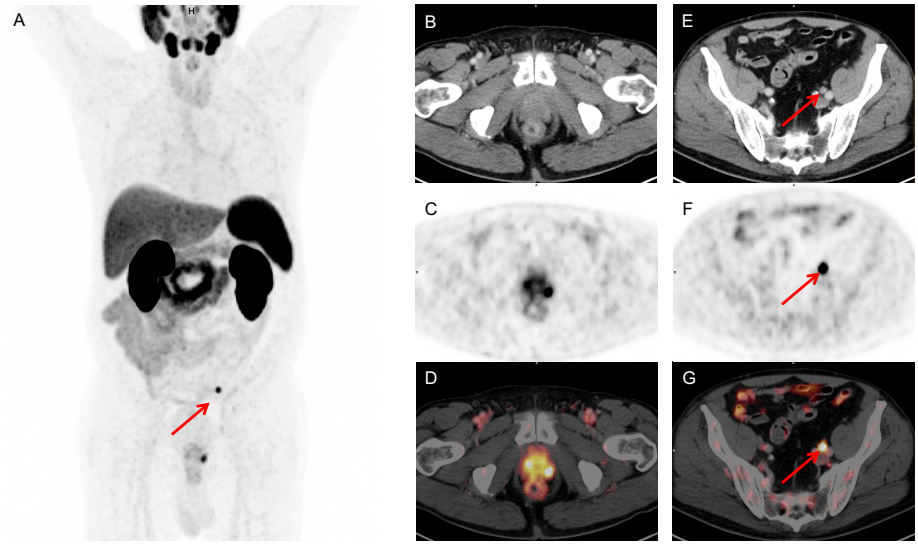

Note. This sample shows the imaging results of a 71-year-old patient with a Gleason score of 10 and an initial prostate-specific antigen level of 1.15 ng/ml. (A) The whole-body maximum-intensity projection displays a local tumour and one suspect lesion (arrow). (B, C, and D) The local tumour is not detectable on CT (B) but shows increased tracer uptake on ^{18}F-rhPSMA-7 PET (C) and PET/CT (D). (E, F, and G) CT (E) reveals a suggestive finding (arrow), with an 8mm

lymph node ventral to left external iliac vein; corresponding ^{18}F- rhPSMA-7 PET (F) and PET/CT images (G) show an intense uptake with high lesion-to-background ratio in this small lymph node, indicating a lymph node metastasis. Radical prostatectomy with extended pelvic lymph node dissection confirmed a single lymph node metastasis.

Figure 11: *ROC curves for ^{18}F-PSMA-7 and morphological imaging*

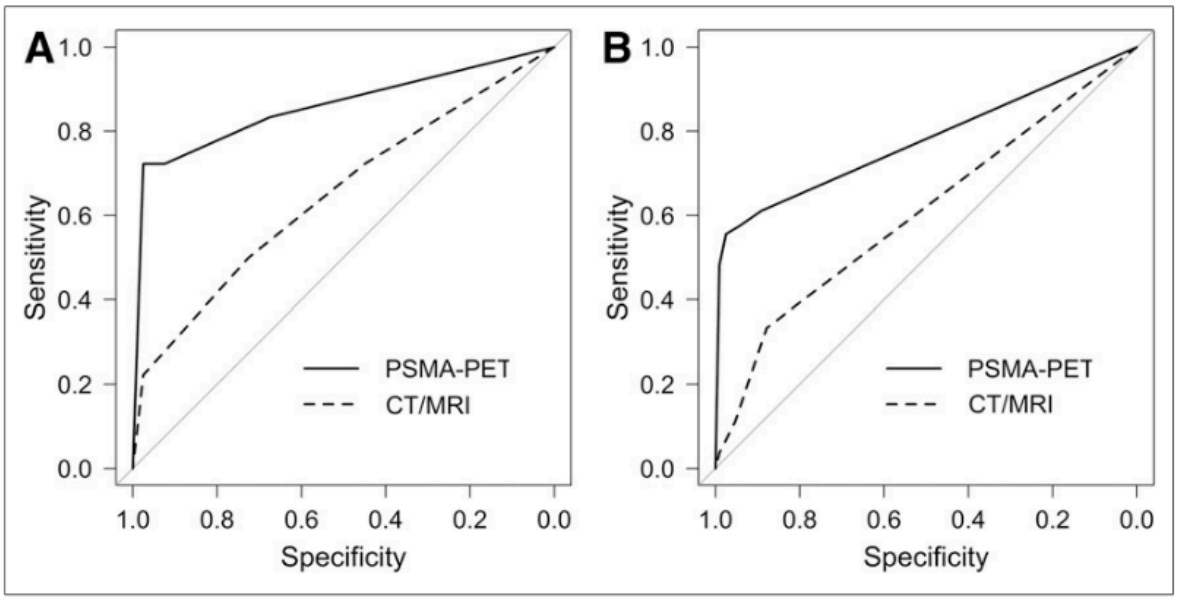

Note. ROC curves for ^{18}F-rhPSMA-7 PET and morphological imaging (MRI/CT) for primary lymph node staging of prostate cancer in patient-based analysis (A) and template-based analysis (B).
A comparison to an AUC of 0.5 is indicated by the grey line.
ROC = receiver-operating-characteristic, AUC = area under the curve, PSMA-PET = prostate-specific membrane antigen positron-emission-tomography. MRI = magnetic resonance imaging, CT = computer tomography.

Diagnostic efficacy in patient-based analysis

With ^{18}F-rhPSMA-7 PET from 18 patients with histologically proven lymph node metastasis 13 were correctly classified as positive, leading to a sensitivity of 72.2% (95% CI, 46.5%–90.3%). From 40 patients without lymph node metastases 37 were correctly claimed as negative on ^{18}F-rhPSMA-7, showing a specificity of 92.5% (95% CI, 79.6%–98.4%). The positive predictive value (PPV) was 81.3%, the negative predictive value (NPV) was 88.1%. In total, ^{18}F-rhPSMA-7 PET showed an accuracy of 86.2% (95% CI, 74.6%– 93.9%) on patient-based analysis (see Table 6).

With morphological imaging alone 9 out of the 18 patients were rated as positive, resulting in a sensitivity of 50.0% (95% CI, 26.0%–74.0%). As 29 patients out of 40 without lymph node metastases were classified as negative a specificity of 72.5% (95% CI, 56.1%–85.4%) was calculated. The PPV was 45.0%, the NPV was 76.3%. In total morphological imaging alone showed an accuracy of 65.5% (95% CI, 51.9%–77.5%) (see Table 7).

In 35 of 58 patients (60.3%) PET and morphological imaging showed concordant correct results (regarding true-positive and true-negative results). In 5 of 58 patients (8.6%) PET and morphological imaging showed concordant incorrect results (regarding false-positive and false-negative). Discordant results were obtained in 18 patients (31.0%). Histological evaluation revealed that PET imaging gave true-positive and true-negative results in 15 of these 18 patients (83.3%) with discordant results. ^{18}F-rhPSMA-7 PET reported both fewer false-positives (3 vs. 11 patients) and fewer false-negatives (5 vs. 9 patients) than morphological imaging.

Table 6*: Diagnostic efficacy of 18F-rhPSMA-7 PET/CT or PET/MRI on patient-based analysis*

Histology of LN metastases			
Grade	Positive	Negative	
1	**13**	1	PPN 81.3%
2	**0**	2	
3	1	**5**	NPV 88.1%
4	1	**5**	
5	3	**27**	
Total	**18**	**40**	**58**
	Sens. 72.2%	Spec. 92.5%	Acc. 86.2%

Note. Results of the calculated sensitivity (Sens.), specificity (Spec.), positive predictive value (PPV), negative predictive value (NPV) and accuracy (Acc.) for ^{18}F-rhPSMA PET on patient-based analysis.

Values for PSMA-PET Grading: 1+2 positive, 3-5: negative for LN metastasis, based on the highest Youden index (sensitivity + specificity - 1).

LN: lymph nodes.

Table 7*: Diagnostic efficacy of morphologic imaging on patient-based analysis*

Histology of LN metastases			
Grade	Positive	Negative	
1	**4**	1	PPN 45.0%
2	**0**	0	
3	**5**	10	
4	4	**11**	NPV 76.3%
5	5	**18**	
Total	**18**	**40**	**58**
	Sens. 50.0%	Spec. 72.5%	Acc. 65.5%

Note. Results of the calculated sensitivity (Sens.), specificity (Spec.), positive predictive value (PPV), negative predictive value (NPV) and accuracy (Acc.) for morphological imaging (including MRI and CT) on patient-based analysis.

Values for morphological grading: 1-3 positive, 4-5 negative, based on the highest Youden index (sensitivity + specificity - 1).

LN: lymph nodes.

Diagnostic efficacy on template-based analysis

With ^{18}F-rhPSMA-7 PET 28 templates out of 52 templates with histologically proven lymph node metastasis were correctly rated as positive, resulting in a sensitivity of 53.8% (95% CI, 41.3%–66.0%). As 313 out of 323 templates without lymph node metastases were rated as negative with ^{18}F-rhPSMA-7 PET the specificity was 96.9% (95% CI, 91.4%–98.9%). The PPV was 73.7%, the NPV was 92.9%. In total, ^{18}F-rhPSMA-7 PET showed an accuracy of 90.9% (95% CI, 85.7%–94.4%) on a template-based analysis, see Table 8.

Morphological imaging alone classified 5 out of 52 with histologically proven lymph node metastases correctly as positive, resulting in a sensitivity of 9.6% (95% CI, 4.5–19.3%). From 323 templates without lymph node metastases 307 were correctly classified as negative, resulting in a specificity of 95.0% (95% CI, 92.2–96.9%). PPV and NPV were 23.8% and 86.7%, respectively. In total morphological imaging showed an accuracy of 83.2% (95% CI, 76.5–88.3%), see Table 9.

Further work-up revealed the median size of lymph node metastases not detected by ^{18}F-rhPSMA-7 PET was 4.5 mm (range: 0.3–15 mm).

Two patients, who were rated incorrectly as positive by ^{18}F-rhPSMA-7 were 4 month later during the follow-up corrected as true positive as one patient had lymph node metastases in a second PLND after persistently elevated PSA levels and in a second patient radiation planning showed, that positive lesions had not been removed in surgery.

Table 8*: Diagnostic efficacy of ^{18}F-rhPSMA-7 PET/CT or PET/MRI on template-based analysis*

	Histology of LN metastases		
Grade	Positive	Negative	
1	**24**	5	PPN 73.7%
2	**4**	5	
3	1	**10**	NPV 92.9%
4	2	**17**	
5	21	**286**	
Total	**52**	**323**	**375**
	Sens. 53.8 %	Spec. 96.9%	Acc. 90.9%

Note. Calculated sensitivity (Sens.), specificity (Spec.), positive predictive value (PPV), negative predictive value (NPV) and accuracy (Acc.) for ^{18}F-rhPSMA PET on template-based analysis.

Values for PSMA-PET Grading: 1+2 positive, 3-5: negative for LN metastasis, based on the highest Youden index.

LN: lymph nodes

Table 9*: Diagnostic efficacy of morphological imaging on template-based analysis*

Histology of LN metastases			
Grade	Positive	Negative	
1	**1**	4	PPN 23.8%
2	**0**	0	
3	**4**	12	
4	11	**25**	NPV 86.7%
5	36	**282**	
Total	**52**	**323**	**375**
	Sens. 9.6%	Spec. 95.0%	Acc. 83.2%

Note. Calculated sensitivity (Sens.), specificity (Spec.), positive predictive value (PPV), negative predictive value (NPV) and accuracy (Acc.) for morphological imaging on template-based analysis.

Values for morphological grading: 1-3 positive, 4-5 negative, based on the highest Youden index.

LN: lymph nodes.

Discussion

This retrospective study with histopathological validation shows a high diagnostic efficacy of the new tracer ^{18}F-rhPSMA-7 for primary lymph node staging with PET/CT or PET/MRI of patients with a primary high-risk prostate cancer. Furthermore, the diagnostic performance proved to be better than the performance of morphological imaging alone, which was so far recommended by most applicable guidelines during this study (AWMF online, 2019; Mottet et al., 2017). In 2021 the guidelines were adjusted, as mentioned earlier (AWMF online, 2021). The gap was widest in the comparison of sensitivity on a template-based analysis, with a sensitivity of 10% for morphological imaging and 54% for ^{18}F-rhPSMA-7 PET scan. The sensitivity on patient-based analysis was 72% for ^{18}F-rhPSMA-7 PET scan and 50% for morphological imaging. For ^{18}F-rhPSMA-7 PET the specificity was 93% on patient-based analysis and 97% on template-based analysis. For morphological imaging the specificity was 73% for patient-based analysis and 95% for template-based analysis. The accuracy of ^{18}F-

rhPSMA-7 PET was 86% and 91%, versus 66% and 83% for morphologic imaging, for patient- and template-based analyses, respectively.

Comparison of study results with literature concerning diagnostic accuracy

With a sensitivity of 72% on patient-based and 54% on template-based analysis and a specificity of 93% on patient- and 97% on template-based analysis the results are comparable with other ^{18}F-PSMA tracers. ^{18}F-PSMA-1007 PET showed a sensitivity of 71% and a specificity of 81% in the study of Kesch et al. (2017). ^{18}F-PSMA-DCFPyL showed a sensitivity of 63% and a specificity of 95%, reported by Bodar et al. (2019) and a sensitivity of 71% and specificity of 89% in the study of Gorin et al. (2018). On the level of individual nodal packets the sensitivity was 67% and the specificity 93% (Gorin et al., 2018).

In comparison with ^{68}Ga-PSMA-11 the results of this study are also equally good. Due to a similar method the results can be best compared with the study of Maurer, Gschwend, et al. (2016) who analysed 130 patients and reported a patient based sensitivity, specificity and accuracy of ^{68}Ga-PSMA-11-PET of 66%, 99% and 89%. Whereas those of morphological imaging were 44%, 85% and 72%, respectively. They dissected 734 lymph node templates, with 117 showing metastases. On template-based analysis the sensitivity, specificity and accuracy of ^{68}Ga-PSMA-PET were 74%, 99% and 95%, those of morphological imaging were 28%, 97% and 86%, respectively. Of course a comparison with literature is not as meaningful as a direct comparison, but the results of this study go in the same direction as the results of Kesch et al. (2017) who showed equally high diagnostic efficacy of ^{18}F-PSMA-1007 and ^{68}Ga-PSMA-11 in the detection of intra-prostatic lesions using both radiotracers within the same patients.

The tumour uptake of the new tracer ^{18}F-rhPSMA-7 is also comparable to ^{68}Ga-PSMA-11 in literature. In this study a high tumour uptake was registered in 98% of patients, whereas in the study of Maurer, Gschwend, et al. (2016) about ^{68}Ga-PSMA-11, 92% showed a moderate or high tumour uptake.

Discussion of false negatives and false positives

For the evaluation of diagnostic efficacy, it is necessary to have a look at benign structures falsely rated as tumour suspicious (false positives) and malign structures, which weren't

detected as tumour manifestations (false negative) and examine possible reasons for the incorrect classification.

In this study 10 out of 323 lymph nodes (3%) showed an increased tracer uptake while being benign. In the study of Maurer, Gschwend, et al. (2016) with ^{68}Ga-PSMA-11 PET only 5 out of 617 (1%) lymph nodes were falsely claimed as suspicious. Therefore, the probability to have a truly positive lymph node, when it was rated as positive was 74% (PPV) in this study and 95% in the study of Maurer, Gschwend et al. (2016).

Hence it seems that ^{68}Galium might lead to less false negative results than ^{18}F-rhPSMA-7. Rauscher, Krönke and König and their working group (Rauscher, Krönke, König, et al., 2020) detected a difference in the same direction for the comparison of ^{18}F-PSMA-1007 and ^{68}Ga-PSMA-11. They were investigating the number of lesions with benign origin with increased tracer uptake of ^{18}F-PSMA-1007 compared to ^{68}Ga-PSMA-11. They matched 204 patients with BCR, who underwent ^{18}F-PSMA-1007 PET (n=102) or ^{68}Ga-PSMA-11 PET scan (n=102) on the basis of various clinical aspects. In their study ^{18}F-PSMA-1007 PET detected 5 times more suspicious truly benign lesions than ^{68}Ga-PSMA-11. Rauscher, Krönke and König (2020) and their colleagues discussed the attribution of the differences to the characteristics of ^{18}Fluor and ^{68}Gallium, such as lower positron energy, longer half-life, higher injected activities and higher internalization rate of ^{18}Fluor. Furthermore, they highlighted various typical pitfalls in the image evaluation of ^{18}F-PSMA-1007 PET. The most frequently pitfall was the tracer accumulation in cervical, coeliac and sacral ganglia. The second most frequently pitfall was an unspecific uptake of ^{18}F-PSMA-1007 in lymph nodes. They suggest taking CT information such as shape and configuration of lymph nodes as well as clinical context e.g., typical patterns of PCa metastases and PSA score into consideration for a correct classification (Rauscher, Krönke, König, et al., 2020).

In 2020 Rauscher, Krönke and Wurzer et al. and in 2021 Kroenke with colleagues additionally analyzed a retrospective matched-pair comparison of ^{18}F-rhPSMA-7 and ^{68}Ga-PSMA-11 (Kroenke et al., 2021; Rauscher, Krönke, Wurzer, et al., 2020). In these studies there was also a considerable number of false positive lesions detected by both tracers, but more frequent with ^{18}F-rhPSMA-7. Considering this, an adequate reader training to avoid these pitfalls is necessary, to still benefit from the logistical and clinical advantages of ^{18}F-rhPSMA-7. For this a look at the EANM standardized reporting guidelines for PSMA-PET (Ceci et al., 2021) might be helpful.

Furthermore, it must be mentioned that in this study the specificity on template-based analysis was slightly underestimated because two templates designated as false-positive were in fact true-positives which was noticed with follow-up data and histopathology as gold standard.

At the same time, it is important to evaluate reasons for the rating of tumour lesions as benign. In this study 24 out of 52 (46%) lymph nodes with metastases were not rated as tumour manifestation. Further work-up revealed the median size of lymph node metastases not detected by ^{18}F-rhPSMA-7 PET was 4.5 mm. In the study of Maurer, Gschwend, et al. (2016) about ^{68}Ga-PSMA-11 PET 31 out of 117 (27%) were false negative with a medium size of 3 +/- 1mm. One reason for missed lymph node metastasis with PSMA tracers might be, that not all PCa and positive lymph nodes seem to overexpress PSMA as can be also seen in the case study of Broos, Kocken, Van Der Zant, Knol, and Wondergem, (2018).

Advantages of PSMA-tracers over morphological imaging

A precise primary staging is essential for the evaluation of the patients prognosis and an optimal treatment. Especially for lymph node staging recommended morphological imaging shows insufficient diagnostic efficacy (Hövels et al., 2008). The classification of lymph nodes only by size is problematic, because about 80% of lymph nodes with metastases are normal sized (Heesakkers et al., 2008; Tiguert et al., 1999). Research about new tracers for PET/CT and PET/MRI wants to overcome this problem, whereby PSMA targeting tracers are especially promising (Eiber et al., 2017). The accumulation of PSMA targeting tracers is independent of the metabolic state (Silver et al., 1997). Furthermore the lesion-to-background ratio as well as the lacking expression of PSMA by normal lymphatic or retroperitoneal fatty tissue are favourable for the detection of metastatic lymph nodes (Silver et al., 1997).

Advantages of the new tracer over ^{68}Ga-PSMA-11

The new tracer ^{18}F-rhPSMA offers some advantages over other PSMA targeting ligands such as ^{68}Ga-PSMA-11 and it already showed promising results in patients with primary high risk prostate cancer and with biochemical recurrence (Eiber et al., 2019; Krönke et al., 2020). The low excretion via the bladder offers a better evaluation of the local tumour and loco-regional

lymph nodes. Nevertheless, it cannot be ruled out, that Furosemid might have influenced this. To evaluate the excretion characteristics further a study with a direct comparison of ^{18}F-rhPSMA with and without the use of diuretics is necessary (Oh et al., 2019). Furthermore ^{18}Fluor shows a longer half-life than ^{68}Gallium (110min vs. 68min) and it can be produced in large-scale with a cyclotron. Those two characteristics offer the possibility of a wide range distribution and the supply of clinics without their own cyclotron (Glatting et al., 2017). Despite the in theory achievable higher image resolution of ^{18}F over ^{68}Ga, the results of this study show comparable results and no superiority of ^{18}F-rhPSMA-7 over ^{68}Ga-PSMA-11 in literature. The difference might become obvious with PET scanners with even higher resolution or in relation with other factors such as PSA score: in the study of patients with recurrent PCa from Eiber et al. (2019) the detection rate of ^{18}F-rhPSMA-7 was increasing with higher PSA levels, but the detection rate of ^{18}F-rhPSMA-7 was higher than the reported detection rate of ^{68}Ga-PSMA-11 in patients with very low PSA levels especially below 0.5 ng/ml. So, the logistical advantages might be more relevant than the image quality benefits compared with ^{68}Ga-PSMA-11 so far. But it is necessary to keep in mind that a comparison with literature allows only limited conclusions.

Whereas in the comparison with ^{18}F-PSMA-1007 and ^{18}F-PSMA-DCFPyL an additional advantage lies in the radiohybrid concept: it offers the opportunity to transfer the knowledge from one biochemical twin to the other (^{18}F-^{nat}Ga-PSMA and ^{19}F-^{68}Ga-PSMA) and the application of a theranostic approach (^{19}F-^{nat}Lu-PSMA and ^{18}F-^{177}Lu-PSMA) (Wurzer, Di Carlo, et al., 2020). The new tracer was licensed to Blue Earth Diagnostic, who are aiming for regulatory approval focusing on the ^{18}F-rhPSMA-7 with a Gallium-complexed chelator.

Limitations of this study

For the interpretation of the results following limitations of this study need to be considered: The study design was retrospective and the comparison with ^{68}Gallium only literature based. Retrospective designs base on a non-randomized patient selection and therefore can lead to biases, such as sample selection biases, which means that only a subgroup of patients takes part in a study and therefore the results are not representative for the whole population (Berk, 1983). But one must also consider that PET and MRI or CT, which were compared directly, took place simultaneously, and therefore a selection bias would affect the diagnostic efficiency results but less the comparison of both modalities. For

a higher representativeness a higher number of patients would have been helpful, especially as lymph node metastases were only in 31% of 58 patients present and therefore the diagnostic efficacy of lymph node detection could be analysed only for 18 patients. Furthermore, the rating could be further improved by more raters and an evaluation of interrater reliability. Histopathology is considered the gold standard in image validation. Due to the impracticability of correlating single lymph nodes with image results, the validation needed to be on a template base. Besides, there was no immunohistochemistry performed for lymph node metastases, but the usually sufficient routine hematoxylin and eosin staining. In addition, the focus was only on lymph node detection and not on the analysis of intraprostatic tumour extent, so no conclusion can be drawn regarding the local tumour. Also bone metastases could not be analysed as only patients with subsequent RP were included and RP is only recommended for localized PCa. The ideal imaging point also can be discussed: Oh et al. (2019) recommend an early imaging point after 50-70 minutes for ^{18}F-rhPSMA-7 to achieve the highest overall image quality. In this study the mean uptake time was 82 minutes, and the range was 60–153 minutes. Ideally the range could be smaller, but practical implementation of an exact imaging point is not always possible. Another aspect which needs consideration is the use of two morphological imaging modalities CT and MRI, which leads to smaller numbers for each modality and only a combined evaluation of performance.

This study should be followed by a prospective study design with randomized assignment to 18F-rhPSMA-7 and 68Ga-PSMA-11 and CT or MRI with a subsequent matching of patients from each group based on clinical information. Rauscher, Krönke, König et al. (2020) and Kroenke with colleagues (2021) analyzed a retrospective matched-pair comparison of ^{18}F-rhPSMA-7 and ^{68}Ga-PSMA-11. With both tracers all primary tumor lesions were detected, whereas slightly more metastatic lesions were observed with ^{68}Ga-PSMA-11 in primary staging (Kroenke et al., 2021; Rauscher, Krönke, König, et al., 2020).

It also needs more research about the potentials of rhPSMA as a theranostic agent for a more personalized therapy. This might become important not only for prostate cancer but other solid tumours, such as renal cell carcinoma (Siva et al., 2020).

Conclusion

The diagnostic efficacy of primary lymph node staging for patients with high-risk prostate carcinoma with the tracer ^{18}F-rhPSMA-7 is superior to morphological imaging and comparable to published data for ^{68}Ga-PSMA-11. Moreover ^{18}F-rhPSMA-7 offers additional logistical, biochemical and economic advantages.

References

amboss.com. (2020). amboss. Retrieved February 18, 2021, from https://next.amboss.com/de/article/dp0ooS?q=prostata#Zbe4c359b1c5a9b39d7c8301e11f263ef

AWMF online. (2019). *Interdisziplinäre Leitlinie der Qualität S3 zur Früherkennung, Diagnose und Therapie der verschiedenen Stadien des Prostatakarzinoms, Kurzversion 5.1*. *AWMF-Register Nr.: 043/022OL*.

AWMF online. (2021). *S3-Leitlinie Prostatakarzinom, Kurzversion 6.2*. *AWMF-Register Nr. 043/022OL*.

Baco, E., Rud, E., Eri, L. M., Moen, G., Vlatkovic, L., Svindland, A., … Ukimura, O. (2016). A randomized controlled rrial to assess and compare the outcomes of two-core prostate biopsy guided by fused magnetic resonance and transrectal ultrasound images and traditional 12-core systematic biopsy. *European Urology*, *69*, 149–156.

Bander, N. H. (2006). Technology insight: Monoclonal antibody imaging of prostate cancer. *Nature Clinical Practice Urology*, *3*, 216–225. https://doi.org/10.1038/ncpuro0452

Berk, R. A. (1983). An introduction to sample selection bias in sociological data. *American Sociological Review*, *48*, 386–398.

Beyer, T., Townsend, D. W., Brun, T., Kinahan, P. E., Charron, M., Roddy, R., … Nutt, R. (2000). A combined PET/CT scanner for clinical oncology. *Journal of Nuclear Medicine*, *41*, 1369–1379.

BioRender.com. (2021). BioRender. Retrieved February 18, 2021, from https://biorender.com/

Bodar, Y. J. L., Jansen, B., Van Der Voorn, P., Zwezerijnen, B., Nieuwenhuijzen, J., Hendrikse, H., … Vis, A. (2019). Detection of intraprostatic tumour localisation with 18F-PSMA PET/CT compared to radical prostatectomy specimens: Is PSMA-targeted biopsy feasible? –the DeTeCT trial–. *European Urology Supplements*, *18*, 3377–3378.

Bostwick, D. G., Pacelli, A., Blute, M., Roche, P., & Murphy, G. P. (1998). Prostate specific membrane antigen expression in prostatic intraepithelial neoplasia and adenocarcinoma: A study of 184 cases. *Cancer*, *82*, 2256–2261.

Brierley, J. D., Gospodarowicz, M. K., & Wittekind, C. (2017). *TNM Classification of malignant tumours*. (Union for international cancer control (UICC), Ed.) (Eight). Oxford: Wiley Blackwell.

Briganti, A., Abdollah, F., Nini, A., Suardi, N., Gallina, A., Capitanio, U., … Montorsi, F. (2012). Performance characteristics of computed tomography in detecting lymph node metastases in contemporary patients with prostate cancer treated with extended pelvic lymph node dissection. *European Urology*, *61*, 1132–1138.

Briganti, A., Larcher, A., Abdollah, F., Capitanio, U., Gallina, A., Suardi, N., … Montorsi, F. (2012). Updated nomogram predicting lymph node invasion in patients with prostate cancer undergoing extended pelvic lymph node dissection: The essential importance of percentage of positive cores. *European Urology*, *61*, 480–487.

Broos, W. A. M., Kocken, M., Van Der Zant, F. M., Knol, R. J. J., & Wondergem, M. (2018). Metastasized 18F-DCFPyL-negative prostatic adenocarcinoma without neuroendocrine differentiation. *Clinical Nuclear Medicine*, *43*, 120–122.

Bubendorf, L., Schöpfer, A., Wagner, U., Sauter, G., Moch, H., Willi, N., … Mihatsch, M. J. (2000). Metastatic patterns of prostate cancer: An autopsy study of 1,589 patients. *Human Pathology*, *31*, 578–583.

Buyyounouski, M. K., Choyke, P. L., McKenney, J. K., Sartor, O., Sandler, H. M., Amin, M. B., … Lin, D. W. (2017). Prostate cancer - major changes in the American Joint Committee on Cancer eighth edition cancer staging manual. *CA: A Cancer Journal for Clinicians*, *67*, 245–253.

Cal-González, J., Herraiz, J. L., España, S., Desco, M., Vaquero, J. J., & Udías, J. M. (2009). Positron range effects in high resolution 3D pet imaging. *IEEE Nuclear Science Symposium Conference Record*, 2788–2791.

Carter, R. E., Feldman, A. R., & Coyle, J. T. (1996). Prostate-specific membrane antigen is a hydrolase with substrate and pharmacologic characteristics of a neuropeptidase. *Neurobiology*, *93*, 749–753.

Castro, E., Goh, C., Olmos, D., Saunders, E., Leongamornlert, D., Tymrakiewicz, M., … Eeles, R. (2013). Germline BRCA mutations are associated with higher risk of nodal involvement, distant metastasis, and poor survival outcomes in prostate cancer. *Journal of Clinical Oncology*, *31*, 1748–1757.

Ceci, F., Oprea-Lager, D. E., Emmett, L., Adam, J. A., Bomanji, J., Czernin, J., … Herrmann, K. (2021). E-PSMA: The EANM standardized reporting guidelines v1.0 for PSMA-PET. *European Journal of Nuclear Medicine and Molecular Imaging*, *48*, 1626–1638.

Chang, S. S., O'Keefe, D. S., Bacich, D. J., Reuter, V. E., Heston, W. D. W., & Gaudin, P. B.

(1999). Prostate-specific membrane antigen is produced in tumor-associated neovasculature. *Clinical Cancer Research*, *5*, 2674–2681.

Clopper, C. J., & Pearson, E. S. (1934). The use of confidence or fiducial limits illustrated in the case of the binomial. *Biometrika*, *26*, 404–413.

Conti, M., & Eriksson, L. (2016). Physics of pure and non-pure positron emitters for PET: A review and a discussion. *EJNMMI Physics*, *3*, 1–17.

Corfield, J., Perera, M., Bolton, D., & Lawrentschuk, N. (2018). 68Ga-prostate specific membrane antigen (PSMA) positron emission tomography (PET) for primary staging of high-risk prostate cancer: A systematic review. *World Journal of Urology*, *36*, 519–527.

D'Amico, A. V, Whittington, R., Malkowicz, S. B., Schultz, D., Blank, K., Broderick, G. A., … Wein, A. (1998). Biochemical outcome after radical prostatectomy, external beam radiation therapy, or interstitial radiation therapy for clinically localized prostate cancer. *JAMA - Journal of the American Medical Association*, *280*, 969–974.

De Jong, H. W. A. M., Perk, L., Visser, G. W. M., Boellaard, R., van Dongen, G. A. M. S., & Lammertsma, A. A. (2005). High resolution PET imaging characteristics of 68-Ga, 124-I and 89-Zr compared to 18-F. *Nuclear Science Symposium Conference Record*, 1624–1627.

DeLong, E. R., DeLong, D. V., & Clarke-Pearson, D. L. (1988). Comparing the areas under two or more correlated receiver operating characteristic curves: A nonparametric approach. *Biometrics*, *44*, 837–845.

Delso, G., Fürst, S., Jakoby, B., Ladebeck, R., Ganter, C., Nekolla, S. G., … Ziegler, S. I. (2011). Performance measurements of the siemens mMR integrated whole-body PET/MR scanner. *Journal of Nuclear Medicine*, *52*, 1914–1922.

Derenzo, S. E. (1986). Mathematical removal of positron range blurring in high resolution tomography. *IEEE Transactions on Nuclear Science*, *33*, 565–569.

Disselhorst, J. A., Brom, M., Laverman, P., Slump, C. H., Boerman, O. C., Oyen, W. J. G., … Visser, E. P. (2010). Image-quality assessment for several positron emitters using the NEMA NU 4-2008 standards in the siemens inveon small-animal PET scanner. *Journal of Nuclear Medicine*, *51*, 610–617.

Eiber, M., Fendler, W. P., Rowe, S. P., Calais, J., Hofman, M. S., Maurer, T., … Giesel, F. L. (2017). Prostate-specific membrane antigen ligands for imaging and therapy. *Journal of Nuclear Medicine*, *58*, 67–76.

Eiber, M., Krönke, M., Wurzer, A., Ulbrich, L., Jooß, L., Maurer, T., … Weber, W. A. (2019). 18 F-rhPSMA-7 positron emission tomography for the detection of biochemical recurrence of prostate cancer following radical prostatectomy. *Journal of Nuclear Medicine*, 1–29.

Eiber, M., Maurer, T., Souvatzoglou, M., Beer, A. J., Ruffani, A., Haller, B., … Schwaiger, M. (2015). Evaluation of hybrid 68Ga-PSMA ligand PET/CT in 248 patients with biochemical recurrence after radical prostatectomy. *Journal of Nuclear Medicine*, *56*, 668–674.

Eiber, M., Weirich, G., Holzapfel, K., Souvatzoglou, M., Haller, B., Rauscher, I., … Maurer, T. (2016). Simultaneous 68Ga-PSMA HBED-CC PET/MRI Improves the localization of primary prostate cancer. *European Urology*, *70*, 829–836.

Esen, T., Kılıç, M., Seymen, H., Acar, Ö., & Demirkol, M. O. (2020). Can Ga-68 PSMA PET/CT replace conventional imaging modalities for primary lymph node and bone staging of prostate cancer? *European Urology Focus*, *6*, 218–220.

Esposito, K., Chiodini, P., Capuano, A., Bellastella, G., Maiorino, M. I., Parretta, E., … Giugliano, D. (2013). Effect of metabolic syndrome and its components on prostate cancer risk: Meta-analysis. *Journal of Endocrinological Investigation*, *36*, 132–139.

Evangelista, L., Guttilla, A., Zattoni, F., Muzzio, P. C., & Zattoni, F. (2013). Utility of choline positron emission tomography/computed tomography for lymph node involvement identification in intermediate- to high-risk prostate cancer: A systematic literature review and meta-analysis. *European Urology*, *63*, 1040–1048.

Fenton, J. J., Weyrich, M. S., Durbin, S., Liu, Y., Bang, H., & Melnikow, J. (2018). Prostate-specific antigen-based screening for prostate cancer evidence report and systematic review for the us preventive services task force. *JAMA - Journal of the American Medical Association*, *319*, 1914–1931.

Ferreira, A. R., Abrunhosa-branquinho, A., Vendrell, I., Quintela, A., Pina, F., & Ribeiro, L. (2015). Prostate Cancer. In *International Manual of Oncology Practice* (pp. 519–554).

Ghosh, A., & Heston, W. D. W. (2004). Tumor target prostate specific membrane antigen (PSMA) and its regulation in prostate cancer. *Journal of Cellular Biochemistry*, *91*, 528–539.

Giesel, F. L., Hadaschik, B., Cardinale, J., Radtke, J., Vinsensia, M., Lehnert, W., … Kratochwil, C. (2017). F-18 labelled PSMA-1007: Biodistribution, radiation dosimetry and histopathological validation of tumor lesions in prostate cancer patients. *European Journal of Nuclear Medicine and Molecular Imaging*, *44*, 678–688.

Giesel, F. L., Will, L., Lawal, I., Lengana, T., Kratochwil, C., Vorster, M., … Sathekge, M. (2018). Intraindividual comparison of 18 F-PSMA-1007 and 18 FDCFPyL PET/CT in the prospective evaluation of patients with newly diagnosed prostate carcinoma: A pilot study. *Journal of Nuclear Medicine*, *59*, 1076–1080.

Glatting, G., Wängler, C., & Wängler, B. (2017). Physikalisch-technische Grundlagen und Tracerentwicklung in der Positronenemissionstomografie. In F. Attenberger, U., Ritter, M., Wenz (Ed.), *MR- und PET-Bildgebung der Prostata* (pp. 19–56). Berlin Heidelberg: Springer-Verlag.

Gleason, D. F. (1992). Histologic grading of prostate cancer: A perspective. *Human Pathology*, *23*, 273–279.

Gorin, M. A., Rowe, S. P., Patel, H. D., Vidal, I., Mana-ay, M., Javadi, M. S., … Allaf, M. E. (2018). Prostate specific membrane antigen targeted 18F-DCFPyL positron emission tomography/computerized tomography for the preoperative staging of high risk prostate cancer: Results of a prospective, phase II, single center study. *Journal of Urology*, *199*, 126–132.

Gusman, M., Aminsharifi, J. A., Peacock, J. G., Anderson, S. B., Clemenshaw, M. N., & Banks, K. P. (2019). Review of 18F-Fluciclovine PET for detection of recurrent prostate cancer. *Radiographics*, *39*, 822–841.

Haffner, M. C., Kronberger, I. E., Ross, J. S., Sheehan, C. E., Zitt, M., Mühlmann, G., … Bander, N. H. (2009). Prostate-specific membrane antigen expression in the neovasculature of gastric and colorectal cancers. *Human Pathology*, *40*, 1754–1761.

Haglind, E., Carlsson, S., Stranne, J., Wallerstedt, A., Wilderäng, U., Thorsteinsdottir, T., … Steineck, G. (2015). Urinary incontinence and erectile dysfunction after robotic versus open radical prostatectomy: A prospective, controlled, nonrandomised trial. *European Urology*, *68*, 216–225.

Halekoh, U., Højsgaard, S., & Yan, J. (2006). The R package geepack for generalized estimating equations. *Journal of Statistical Software*, *15*, 1–11.

Hayes, J. H., & Barry, M. J. (2014). Screening for prostate cancer with the prostate-specific antigen test: A review of current evidence. *JAMA - Journal of the American Medical Association*, *311*, 1143–1149.

Heck, M. M., Retz, M., Bandur, M., Souchay, M., Vitzthum, E., Weirich, G., … Nawroth, R. (2014). Topography of lymph node metastases in prostate cancer patients undergoing

radical prostatectomy and extended lymphadenectomy: Results of a combined molecular and histopathologic mapping study. *European Urology*, *66*, 222–229.

Heesakkers, R. A., Hövels, A. M., Jager, G. J., van den Bosch, H. C., Witjes, J. A., Raat, H. P., … Barentsz, J. (2008). MRI with a lymph-node-specific contrast agent as an alternative to CT scan and lymph-node dissection in patients with prostate cancer: A prospective multicohort study. *The Lancet Oncology*, *9*, 850–856.

Hemminki, K. (2012). Familial risk and familial survival in prostate cancer. *World Journal of Urology*, *30*, 143–148.

Hofman, M. S., Lawrentschuk, N., Francis, R. J., Tang, C., Vela, I., Thomas, P., … Murphy, D. G. (2020). Prostate-specific membrane antigen PET-CT in patients with high-risk prostate cancer before curative-intent surgery or radiotherapy (proPSMA): A prospective, randomised, multicentre study. *The Lancet*, *395*, 1208–1216.

Höhne, A., Mu, L., Honer, M., Schubiger, P. A., Ametamey, S. M., Graham, K., … Srinivasan, A. (2008). Synthesis, 18F-labeling, and in vitro and in vivo studies of bombesin peptides modified with silicon-based building blocks. *Bioconjugate Chemistry*, *19*, 1871–1879.

Holmberg, L., Bill-Axelson, A., Steineck, G., Garmo, H., Palmgren, J., Johansson, E., … Johansson, J. E. (2012). Results from the scandinavian prostate cancer group trial number 4: A randomized controlled trial of radical prostatectomy versus watchful waiting. *Journal of the National Cancer Institute - Monographs*, *2011*, 230–233.

Hope, T. A., Goodman, J. Z., Allen, I. E., Calais, J., Fendler, W. P., & Carroll, P. R. (2019). Metaanalysis of 68Ga-PSMA-11 PET accuracy for the detection of prostate cancer validated by histopathology. *Journal of Nuclear Medicine*, *60*, 786–793.

Horoszewicz, J. S., Leong, S. S., Kawinski, E., Karr, J. P., Rosenthal, H., Chu, T. M., … Murphy, G. P. (1983). LNCaP model of human prostatic carcinoma. *Cancer Research*, *43*, 1809–1818.

Hövels, A. M., Heesakkers, R. A. M., Adang, E. M., Jager, G. J., Strum, S., Hoogeveen, Y. L., … Barentsz, J. O. (2008). The diagnostic accuracy of CT and MRI in the staging of pelvic lymph nodes in patients with prostate cancer: a meta-analysis. *Clinical Radiology*, *63*, 387–395.

Jadvar, H. (2013). Imaging evaluation of prostate cancer with 18F- fluorodeoxyglucose PET/CT: Utility and limitations. *European Journal of Nuclear Medicine and Molecular Imaging*, *40*, 8–13.

Kasivisvanathan, V., Rannikko, A. S., Borghi, M., Panebianco, V., Mynderse, L. A., Vaarala, M. H., … Bjartell, A. (2018). MRI-targeted or standard biopsy for prostate-cancer diagnosis. *New England Journal of Medicine*, *378*, 1767–1777.

Keam, S. J. (2021). Piflufolastat F 18: Diagnostic first approval. *Molecular Diagnosis and Therapy*, *25*, 647–656.

Kesch, C., Vinsensia, M., Radtke, J. P., Schlemmer, H. P., Heller, M., Ellert, E., … Giesel, F. L. (2017). Intraindividual comparison of18F-PSMA-1007 PET/CT, multiparametric MRI, and radical prostatectomy specimens in patients with primary prostate cancer: A retrospective, proof-of-concept study. *Journal of Nuclear Medicine*, *58*, 1805–1810.

Kotasidis, F. A., Angelis, G. I., Anton-Rodriguez, J., Matthews, J. C., Reader, A. J., & Zaidi, H. (2014). Isotope specific resolution recovery image reconstruction in high resolution PET imaging. *Medical Physics*, *41*, 1–11.

Kroenke, M., Mirzoyan, L., Horn, T., Peeken, J. C., Wurzer, A., Wester, H.-J., … Rauscher, I. (2021). Matched-pair comparison of 68Ga-PSMA-11 and 18F-rhPSMA-7 PET/CT in patients with primary and biochemical recurrence of prostate cancer: Frequency of non–tumor-related uptake and tumor positivity. *Journal of Nuclear Medicine*, *62*, 1082–1088.

Krönke, M., Wurzer, A., Schwamborn, K., Ulbrich, L., Jooß, L., Maurer, T., … Eiber, M. (2020). Histologically-confirmed diagnostic efficacy of 18 F-rhPSMA-7 positron emission tomography for N-staging of patients with primary high risk prostate cancer. *Journal of Nuclear Medicine*, *61*, 710–715.

Kuten, J., Fahoum, I., Savin, Z., Shamni, O., Gitstein, G., Hershkovitz, D., … Even-Sapir, E. (2019). Head-to head comparison of 68Ga-PSMA-11 with 18F-PSMA-1007 PET/CT in staging prostate cancer using histopathology and immunohistochemical analysis as reference-standard. *Journal of Nuclear Medicine*, 1–27.

Lengana, T., Lawal, I. O., Boshomane, T. G., Popoola, G. O., Mokoala, K. M. G., Moshokoa, E., … Sathekge, M. M. (2018). 68Ga-PSMA PET/CT replacing bone scan in the initial staging of skeletal metastasis in prostate cancer: A fait accompli? *Clinical Genitourinary Cancer*, *16*, 392–401.

Levin, C. S., & Hoffman, E. J. (1999). Calculation of positron range and its effect on the fundamental limit of positron emission tomography system spatial resolution. *Physics in Medicine and Biology*, *44*, 781–799.

Lin, C. Y., Lee, M. T., Lin, C. L., & Kao, C. H. (2019). Comparing the staging/restaging performance of 68Ga-labeled prostate-specific membrane antigen and 18F-Choline PET/CT in prostate cancer: A systematic review and meta-analysis. *Clinical Nuclear Medicine*, *44*, 365–376.

Liu, I. J., Zafar, M. B., Lai, Y. H., Segall, G. M., & Terris, M. K. (2001). Fluorodeoxyglucose positron emission tomography studies in diagnosis and staging of clinically organ-confined prostate cancer. *Urology*, *57*, 108–111.

Mason, N. S., & Mathis, C. A. (2005). Radiohalogens for PET imaging. In D. L. Bailey, D. W. Townsend, P. E. Valk, & M. N. Maisey (Eds.), *Positron Emission Tomography* (pp. 203–222).

Maurer, T., Eiber, M., Schwaiger, M., & Gschwend, J. E. (2016). Current use of PSMA-PET in prostate cancer management. *Nature Reviews Urology*, *13*, 226–235.

Maurer, T., Gschwend, J. E., Rauscher, I., Souvatzoglou, M., Haller, B., Weirich, G., … Eiber, M. (2016). Diagnostic efficacy of 68Gallium-PSMA positron emission tomography compared to conventional imaging for lymph node staging of 130 consecutive patients with intermediate to high risk prostate cancer. *Journal of Urology*, *195*, 1436–1442.

McNeal, J. E. (1981). The zonal anatomy of the prostate. *The Prostate*, *2*, 35–49.

Meikle, S. R., & Badawi, R. D. (2006). Quantitative Techniques in PET. In *Positron Emission Tomography. Basic Science* (pp. 93–126).

Mesters, J. R., Barinka, C., Li, W., Tsukamoto, T., Majer, P., Slusher, B. S., … Hilgenfeld, R. (2006). Structure of glutamate carboxypeptidase II, a drug target in neuronal damage and prostate cancer. *The EMBO Journal*, *25*, 1375–1384.

Mottet, N., Bellmunt, J., Bolla, M., Briers, E., Cumberbatch, M. G., De Santis, M., … Cornford, P. (2017). EAU-ESTRO-SIOG Guidelines on prostate cancer. Part 1: Screening, diagnosis, and local treatment with curative intent. *European Urology*, *71*, 618–629.

Nanni, C., Schiavina, R., Brunocilla, E., Boschi, S., Borghesi, M., Zanoni, L., … Fanti, S. (2015). 18F-Fluciclovine PET/CT for the detection of prostate cancer relapse: A comparison to 11C-Choline PET/CT. *Clinical Nuclear Medicine*, *40*, e386–e391.

Nanni, C., Zanoni, L., Pultrone, C., Schiavina, R., Brunocilla, E., Lodi, F., … Fanti, S. (2016). 18F-FACBC (anti1-amino-3-18F-fluorocyclobutane-1-carboxylic acid) versus 11C-choline PET/CT in prostate cancer relapse: Results of a prospective trial. *European Journal of Nuclear Medicine and Molecular Imaging*, *43*, 1601–1610.

National Center for Biotechnology Information. (2021). PubChem Compound Summary for CID 7015704, Glu-lys. Retrieved February 18, 2021, from https://pubchem.ncbi.nlm.nih.gov/compound/Glu-lys

Obuchowski, N. A. (1997). Nonparametric analysis of clustered ROC curve data. *Biometrics*, *53*, 567–578.

Oh, S. W., Wurzer, A., Teoh, E. J., Oh, S., Langbein, T., Krönke, M., … Eiber, M. (2019). Quantitative and qualitative analyses of biodistribution and PET image quality of novel radiohybrid PSMA, 18F- rhPSMA-7, in patients with prostate cancer. *Journal of Nuclear Medicine*, jnumed.119.234609.

Okarvi, S. M. (2019). Recent developments of prostate-specific membrane antigen (PSMA)-specific radiopharmaceuticals for precise imaging and therapy of prostate cancer: An overview. *Clinical and Translational Imaging*, *7*, 189–208.

Paul, R., Zimmermann, F., Dettmar, P., Adam, M., van Randenborgh, H., Alschibaja, M., … Seitz, M. (2008). Prostatakarzinom. In T. M. Treiber, U., Zaak, D. (Ed.), *Manual Urogenitale Tumore* (4th ed., pp. 1–82). München: W. Zuckschwerdt Verlag.

Perera, M., Papa, N., Roberts, M., Williams, M., Udovicich, C., Vela, I., … Murphy, D. G. (2019). Gallium-68 prostate-specific membrane antigen positron emission tomography in advanced prostate cancer - Updated diagnostic utility, sensitivity, specificity, and distribution of prostate-specific membrane antigen-avid lesions: A systematic review and met. *European Urology*, 1–15.

Quick, H. H., Von Gall, C., Zeilinger, M., Wiesmüller, M., Braun, H., Ziegler, S., … Lell, M. (2013). Integrated whole-body PET/MR hybrid imaging: Clinical experience. *Investigative Radiology*, *48*, 280–289.

R Core Team. (2020). The R project for statistical computing. Retrieved March 10, 2020, from https://www.r-project.org/

Rajasekaran, S. A., Anilkumar, G., Oshima, E., Bowie, J. U., Liu, H., Heston, W., … Rajasekaran, A. K. (2003). A novel cytoplasmic tail MCCCL motif mediates the internalization of prostate-specific membrane antigen. *Molecular Biology of the Cell*, *14*, 4835–4845.

Rauscher, I., Krönke, M., König, M., Gafita, A., Maurer, T., Horn, T., … Eiber, M. (2020). Matched-pair comparison of 68Ga-PSMA-11 PET/CT and 18F-PSMA-1007 PET/CT: Frequency of pitfalls and detection efficacy in biochemical recurrence after radical prostatectomy. *Journal of Nuclear Medicine*, *61*, 51–57.

Rauscher, I., Krönke, M., Wurzer, A., Wester, H., Weber, W., & Eiber, M. (2020). Matched-pair comparison of 68Ga-PSMA-11 and 18F-rhPSMA-7 PET/CT in patients with primary and biochemical recurrent prostate cancer. *Journal of Nuclear Medicine*, *61*(supplement 1), 42.

Rautio, A., Kivi, M., Poksi, A., & Šamarina, G. (2019). Diagnostic performance and impact on management intent of 18F-PSMA-1007 PET/CT in newly diagnosed high-risk prostate cancer. *European Urology Supplements*, *18*, e3457.

Robin, X., Turck, N., Hainard, A., Tiberti, N., Lisacek, F., Sanchez, J. C., & Müller, M. (2011). pROC: An open-source package for R and S+ to analyze and compare ROC curves. *BMC Bioinformatics*, *12*, 1–8.

Samplaski, M. K., Heston, W., Elson, P., Magi-Galluzzi, C., & Hansel, D. E. (2011). Folate hydrolase (prostate-specific antigen) 1 expression in bladder cancer subtypes and associated tumor neovasculature. *Modern Pathology*, *24*, 1521–1529.

Sánchez-Crespo, A., Andreo, P., & Larsson, S. A. (2004). Positron flight in human tissues and its influence on PET image spatial resolution. *European Journal of Nuclear Medicine and Molecular Imaging*, *31*, 44–51.

Schulte, E. (2020). Männliches Genitale. In G. Aumüller, G. Aust, A. Conrad, J. Engele, J. Kirsch, G. Maio, … L. J. Wurzinger (Eds.), *Duale Reihe Anatomie* (5th ed., pp. 826–848). Stuttgart: Thieme.

Schwarzenboeck, S. M., Rauscher, I., Bluemel, C., Fendler, W. P., Rowe, S. P., Pomper, M. G., … Eiber, M. (2017). PSMA ligands for PET imaging of prostate cancer. *Journal of Nuclear Medicine*, *58*, 1545–1552.

Silver, D. A., Pellicer, I., Fair, W. R., Heston, W. D. W., & Cordon-Cardo, C. (1997). Prostate-specific membrane antigen expression in normal and malignant human tissues. *Clinical Cancer Research*, *3*, 81–85.

Siva, S., Udovicich, C., Tran, B., Zargar, H., Murphy, D. G., & Hofman, M. S. (2020). Expanding the role of small-molecule PSMA ligands beyond PET staging of prostate cancer. *Nature Reviews Urology*, *17*, 107–118.

Smith, P. J., & Hadgu, A. (1992). Sensitivity and specificity for correlated observations. *Statistics in Medicine*, *11*, 1503–1509.

Soderlund, A. T., Chaal, J., Tjio, G., Totman, J. J., Conti, M., & Townsend, D. W. (2015). Beyond 18F-FDG: Characterization of PET/CT and PET/MR scanners for a

comprehensive set of positron emitters of growing application-18F, 11C, 89Zr, 124I,68Ga, and 90Y. *Journal of Nuclear Medicine*, *56*, 1285–1291.

Souvatzoglou, M., Eiber, M., Martinez-Moeller, A., Fürst, S., Holzapfel, K., Maurer, T., … Beer, A. J. (2013). PET/MR in prostate cancer: Technical aspects and potential diagnostic value. *European Journal of Nuclear Medicine and Molecular Imaging*, *40*, 79–88.

Spohn, F., Radtke, J. P., Düwel, C., Eiber, M., Körber, S., Gasch, C., … Giesel, F. L. (2019). Aktueller Stand der PSMA-PET-Diagnostik beim Prostatakarzinom. *Radiopraxis*, *12*, 1–14.

Tiffany, C. W., Lapidus, R. G., Merion, A., Calvin, D. C., & Slusher, B. S. (1999). Characterization of the enzymatic activity of PSM: Comparison with brain NAALADase. *The Prostate*, *39*, 28–35.

Tiguert, R., Gheiler, E. L., Tefilli, M. V., Oskanian, P., Banerjee, M., Grignon, D. J., … Wood, D. P. (1999). Lymph node size does not correlate with the presence of prostate cancer metastasis. *Urology*, *53*, 367–371.

Tolvanen, T., Kalliokoski, K. K., Malaspina, S., Kuisma, A., Lahdenpohja, S., Postema, E. J., … Scheinin, M. (2021). Safety, biodistribution and radiation dosimetry of 18 F-rhPSMA-7.3 in healthy adult volunteers. *Journal of Nuclear Medicine*, *62*, 679–684.

Torre, L. A., Bray, F., Siegel, R. L., Ferlay, J., Lortet-Tieulent, J., & Jemal, A. (2015). Global Cancer Statistics, 2012. *CA: A Cancer Journal of Clinicians.*, *65*, 87–108.

U.S. Food and Drug Administration. (2012). FDA approves 11C-Choline for PET in prostate cancer. *Journal of Nuclear Medicine*, *53*, 11N.

U.S. Food and Drug Administration. (2016). FDA approves new diagnostic imaging agent to detect recurrent prostate cancer. Retrieved December 2, 2021, from https://www.fda.gov/news-events/press-announcements/fda-approves-new-diagnostic-imaging-agent-detect-recurrent-prostate-cancer

U.S. Food and Drug Administration. (2020). FDA approves first PSMA-targeted PET imaging drug for men with prostate cancer. Retrieved December 2, 2021, from https://www.fda.gov/news-events/press-announcements/fda-approves-first-psma-targeted-pet-imaging-drug-men-prostate-cancer

U.S. Food and Drug Administration. (2021). FDA approves second PSMA-targeted PET imaging drug for men with prostate cancer. Retrieved December 2, 2021, from https://www.fda.gov/drugs/news-events-human-drugs/fda-approves-second-psma-

targeted-pet-imaging-drug-men-prostate-cancer

van Leeuwen, P. J., Emmett, L., Ho, B., Delprado, W., Ting, F., Nguyen, Q., & Stricker, P. D. (2017). Prospective evaluation of 68Gallium-prostate-specific membrane antigen positron emission tomography/computed tomography for preoperative lymph node staging in prostate cancer. *BJU International*, *119*, 209–215.

Wallis, C. J. D., Mahar, A. L., Choo, R., Herschorn, S., Kodama, R. T., Shah, P. S., … Nam, R. K. (2016). Second malignancies after radiotherapy for prostate cancer: Systematic review and meta-analysis. *BMJ (Online)*, *352*, 1–11.

Wurzer, A., Di Carlo, D., Herz, M., Richter, A., Robu, S., Schirrmacher, R., … Wester, H. (2021). Automated synthesis of [18F]Ga-rhPSMA-7/ -7.3: Results, quality control and experience from more than 200 routine productions. *EJNMMI Radiopharmacy and Chemistry*, *6*, 1–15.

Wurzer, A., Di Carlo, D., Schmidt, A., Beck, R., Eiber, M., Schwaiger, M., & Wester, H. J. (2020). Radiohybrid ligands: A novel tracer concept exemplified by 18F- or 68Ga-labeled rhPSMA inhibitors. *Journal of Nuclear Medicine*, *61*, 735–742.

Wurzer, A., Parzinger, M., Konrad, M., Beck, R., Günther, T., Felber, V., … Wester, H. J. (2020). Preclinical comparison of four [18F, natGa]rhPSMA-7 isomers: Influence of the stereoconfiguration on pharmacokinetics. *EJNMMI Research*, *10*, 1–10.

Yusufi, N., Wurzer, A., Herz, M., Calogero, A., Feuerecker, B., Weber, W. A., … Eiber, M. (2021). Comparative preclinical biodistribution, dosimetry and endoradiotherapy in mCRPC using 19F/177Lu-rhPSMA-7.3 and 177Lu-PSMA I&T. *Journal of Nuclear Medicine*, *62*, 1106–1111.

Zeger, S. L., & Liang, K.-Y. (1986). Longitudinal data analysis for discrete and continuous outcomes. *Biometrics*, *42*, 121–130.

Zentrum für Krebsregisterdaten und Gesellschaft der epidemiologischen Krebsregister in Deutschland e.V. (2017). *Krebs in Deutschland für 2013/2014* (11th ed.). Berlin: Robert Koch-Institut.

Zuckier, L. S., & DeNardo, G. L. (1997). Trials and tribulations: Oncological antibody imaging comes to the fore. *Seminars in Nuclear Medicine*, *27*, 10–29.